PRODUCTION AND CHARACTERIZATION OF NANO SILVER OXIDE FOR SILVER ZINC BATTERIES

A THESIS SUBMITTED TO
THE GRADUATE SCHOOL OF NATURAL AND APPLIED SCIENCES
OF
MIDDLE EAST TECHNICAL UNIVERSITY

BY

ÖZÜM ÖYKÜM YURTSEVEN

IN PARTIAL FULFILLMENT OF THE REQUIREMENT
FOR
THE DEGREE OF MASTER OF SCIENCE
IN
MICRO AND NANOTECHNOLOGY

AUGUST 2013

Approval of the thesis:

PRODUCTION AND CHARACTERIZATION OF NANO SILVER OXIDE FOR SILVER ZINC BATTERIES

submitted by **ÖZÜM ÖYKÜM YURTSEVEN** in partial fulfillment of the requirements for the degree of **Master of Science in Micro and Nanotechnology Department, Middle East Technical University** by,

Prof. Dr. Canan ÖZGEN _____
Dean, Graduate School of **Natural and Applied Sciences**

Prof. Dr. Tayfun AKIN _____
Head of Department, **Micro and Nanotechnology**

Prof. Dr. M. Kadri AYDINOL _____
Supervisor, **Metallurgical& Materials Eng. Dept., METU**

Assist. Prof. Dr. Emren Nalbant ESENTÜRK _____
Co-Supervisor, **Chemistry Dept., METU**

Examining Committee Members:

Prof. Dr. M. Kadri AYDINOL _____
Metallugical & Materials Eng. Dept., Micro and Nanotechnology, METU

Assist. Prof. Dr. Emren NALBANT ESENTÜRK _____
Chemistry Dept., Micro and Nanotechnology, METU

Assoc Prof. Dr. Caner DURUCAN _____
Metallugical & Materials Eng. Dept., Micro and Nanotechnology, METU

Assist. Prof. Dr. Yener KURU _____
Metallugical & Materials Eng Dept., METU

Assist. Prof. Dr. Y. Eren KALAY
Metallugical & Materials Eng Dept., METU _____

Date: 21/08/2013

I hereby declare that all information in this document has been obtained and presented in accordance with academic rules and ethical conduct. I also declare that, as required by these rules and conduct, I have fully cited and referenced all material and results that are not original to this work.

Name, Last name: ÖZÜM ÖYKÜM YURTSEVEN

Signature:

ABSTRACT

PRODUCTION AND CHARACTERIZATION OF NANO SILVER OXIDE FOR SILVER ZINC BATTERIES

Yurtseven, Özüm Öyküm

M.S., Department of Micro and Nanotechnology

Supervisor: Prof. Dr. M. Kadri Aydinol

Co-Supervisor: Assist. Prof. Dr. Emren Nalbant Esentürk

August 2013, 51 pages

Rechargeable silver-zinc batteries have aroused interest and find various area of usage depending on their notably technical advantages over other battery systems including their high specific energy and high recharge efficiency. In this battery chemistry, silver oxide and metallic zinc are used as the positive and negative active materials respectively. Chemically stabilized particles with large surface areas are needed to reach high discharge rates for battery applications. The use of nanoparticles as electrode materials has made a significant improvement in battery performance due to their enhanced electrical and chemical properties.

In current study, we have successfully synthesized AgO nanoparticles through a sonochemical route. Parametric study was performed to examine the effect of reaction parameters such as reaction time, reaction temperature, and surfactant concentration on the quality of products. Synthesized AgO powder was characterized by particle size analyzer, X-ray diffraction (XRD), and scanning electron microscope (SEM). The AgO content of the prepared powder was 100 % and powder particle size mainly distribute in the range of 100-300 nm.

Keywords: silver oxide zinc battery, AgO nanopowder, sonochemical method

ÖZ

GÜMÜŞ OKSİT ÇİNKO BATARYALAR İÇİN NANO BOYUTTA GÜMÜŞ OKSİT ÜRETİMİ VE KARAKTERİZASYONU

Yurtseven, Özüm Öyküm

Yüksek Lisans, Mikro ve Nanoteknoloji Bölümü

Tez Yöneticisi: Prof. Dr. M. Kadri Aydınol

Ortak Tez Yöneticisi:Y. Doç. Dr. Emren Nalbant Esentürk

Ağustos 2013, 51 sayfa

Yüksek spesifik enerji ve enerji yoğunluğu, yüksek güçlü deşarj kapasitesi ve yüksek şarj edilebilirlik verimlilikleri gibi sundukları avantajlar nedeni ile şarj edilebilir gümüş oksit-çinko bataryalar birçok farklı uygulama alanı bulmuşlardır. Bu pil kimyasında, gümüş oksit ve metalik çinko, sırasıyla pozitif ve negatif aktif madde olarak kullanılmaktadır. Bahsi geçen aktif malzemelerin geniş yüzey alanına sahip ve kimyasal olarak stabil partiküller olması, batarya uygulamalarında yüksek deşarj hızlarına ulaşmak için büyük önem teşkil etmektedir. Yüksek yüzey alanına sahip olmalarından dolayı gelişmiş elektriksel ve kimyasal özellikleriyle nanopartiküllerin elektrot aktif malzemesi olarak kullanımı batarya performansında ve kapasitesinde fark edilir derecede bir iyileşme sağlamaktadır.

Bu çalışmada sono-kimyasal yöntemler kullanarak nano boyutta divalent gümüş oksit üretimi gerçekleştirilmiştir. Yüzey aktif madde konsantrasyonu, reaksiyon zamanı ve sıcaklığın ürünün kalitesine etkisini araştırmak için parametrik çalışma yapılmıştır. Ürünlerin detaylı karakterizasyon çalışmaları taramalı elektron mikroskobu (SEM), X-ışını kırınım yöntemi (XRD) ve parçacık boyut analiz cihazı aracılığı ile yapılmıştır. Analiz sonuçları uygun koşullarda AgO nanopartiküllerin AgO içeriği 100 % olarak tespit edilmiştir ve toz partikül büyüklüğü ağırlıklı olarak 100-300 nm aralığında bir dağılım sergilemiştir.

ANAHTAR KELİMELER: Gümüş oksit çinko batarya, AgO nanotoz, sonokimyasal yöntem

To the memory of my father,

My hero, my role model, and guardian angel …

TURGAY ÇELİK YURTSEVEN

1 May 1954 - 21 October 2007

I am never without you…

ACKNOWLEDGMENTS

I would like to express my sincere gratitude to my supervisor, Prof. Dr. Kadri Aydınol, for his relentless encouragement, faith, constructive guidance and words of motivation throughout the duration of this research study and moreover for the inspiration he provided to ensure the completion of this work. In addition, I would also like to express my thanks to my co-advisor, Assist. Prof. Dr. Emren Nalbant Esentürk, for sharing her knowledge and talents with me and for her generous donation of her time and experience.

I would like to acknowledge and thank to TR Teknoloji for providing me so generously with the financial support needed to conduct the research for this thesis.

I am also grateful to my friend Elçin Dertli for her endless help. Throughout all of the master period, she provided encouragement, sound advice, good company, and lots of good ideas and I would have been lost without her.

Most of all, I also thank my wonderful best friend Gökben Özzaman and all of my great friends, Nur Kader Göleç, Umut Ekiz, Gamze Özer, İlhan Arslanoğlu, Oğuzhan Katlı, Mustafa Can Kaplan, Burcu Kartal and Özgür Kazar for their unwavering friendship, support, encouragement and motivation throughout my undergraduate and graduate studies.

Words fail me to express my appreciation to Sefa Soysal whose dedication, love and persistent confidence in me, has taken the load off my shoulder. I owe him for being unselfishly let his intelligence, passions, and ambitions collide with mine and for making so many things possible.

Finally, I thank my father, Turgay Çelik Yurtseven, my mother, Seval Yurtseven, my brother, Yağız Yiğit Yurtseven, my grandmother, Pervin Oktay, and my grandfather Feridun Oktay, for their endless love and support in every moment of my life. Without my family, this thesis would not have been possible.

TABLE OF CONTENTS

LIST OF FIGURES

FIGURES

LIST OF TABLES

TABLES

CHAPTER 1

INTRODUCTION

Studies on nano materials have become the target of major interest in modern science. Nano materials exhibit unique chemical, mechanical, thermal, magnetic, optical and quantum size effect properties in comparison with their bulk counterparts as a result of their high surface-area-to-volume ratio. When used as battery active materials, these size-dependent fascinating properties of nano materials allow efficient energy storage. They can change conventional batteries characteristics in the direction of greater power densities and higher reliability, lead to better and smaller battery designs. In particular, due to its high theoretical voltage, high energy density, high conductivity and low specific resistance, divalent silver oxide (AgO) nanoparticles have found to be of great interest for the battery applications where critical space, low weight and high power is required.

Several methods have been used and developed for synthesizing crystalline oxide powders in nanoscale dimensions. In literature, two methods are commonly used for preparation of AgO; (i) Electrochemical Preparation (EP) Method, and (ii) Chemical Precipitation (CP) Method. The electrochemical preparation method involves electrochemical oxidation of silver metal in alkaline solutions. It is a lengthy and complicated approach for synthesizing divalent silver oxide nanoparticles. This method is a high cost procedure and results with low purity. Product has a non-uniform stoichiometry (Ag2O/AgO mixture); therefore time consuming purification steps are required.

On the other hand, chemical precipitation process is a very promising way to synthesize AgO particles with gram quantities and high purity. The chemical precipitation method is based on the alkaline oxidation of solutions of Ag (I) salts with ozone or per sulfates. This method is more preferable than electrochemical method because it is a straightforward, low cost, high yield method with narrow size distribution. It has the advantage of precise control over the size and shape properties of nanomaterial in molecular level. Moreover, it is an easy scale up process for production of large volumes of AgO particles in relatively short time.

Metal oxides can be synthesized by all known wet chemical methods but to tailor the particle size in nano range and morphology towards a particular application still remains a challenging task. Chemically stabilized particles with large surface areas are needed to reach

high discharge rates for battery applications. Therefore, preventing particles from agglomeration plays a key role during the whole production process. Generally, surfactants are used to inhibit the coalescence of the particles. That is the rationale behind studying chemical reduction of AgO with using different surfactant chemistries in this thesis work.

After observing the effects of surfactants on mean particle size and particle size distribution, the studies are focused on understanding the effect of the sonocrystallization on morphology, structure and size of the particles. Sonocrystallization is the application of high intensity, low frequency ultrasound to a reaction that allows complete control on crystallization. Increase in reproducibility, decrease in crystal growth rate and particle size are reported effects of sonocrystallization in literature. The use of ultrasound in the synthesis of metal oxides has some promise as well. In addition to advantages listed above, AgO nanoparticles would have a greater uniformity, a higher discharge efficiency, and no trace of the objectionable initial high voltage 'hump' of the conventional electroformed positive electrode. Therefore, the research pioneer of this study is to produce nano-sized divalent silver oxide particles with high speed charge/discharge ability as cathode active material for Zn-AgO battery by both chemical and sonochemical methods. The produced oxide is characterized structurally. To sum up, this study reports the synthesis and characterization of nano-structured crystalline AgO.

CHAPTER 2

LITERATURE REVIEW

2.1 Introduction to Battery Technology

Batteries are technological devices that convert the chemical energy in its active materials directly to electrical energy by chemical reactions taking place in electrodes. In batteries, active material in the electrodes runs the electrochemical reactions. These chemical reactions require the transfer of electrons from one electrode to another by an electric circuit created with the help of the electrolyte. Batteries are very common power source for domestic, industrial, military and aerospace applications [1, 2].

Although the phrase "battery" is usually employed, actually the "cell" is the main assembly where the electricity is created. The basic member of each battery is called "the cell". Cell is a basic electrochemical unit, and the battery is an assembly of several cells. To distinguish the differences between a battery and a cell, one should think of that a battery is generated by linking cells in parallel, in series, or both, with respect to the desired output voltage and capacity. The cell consists of four basic components [3]. Figure 1 shows the components of a cell. The voltage, measured in volts and symbolized as (V), is the electrical energy that it gives off. The current, measured in amperes and symbolized as (A), is the rate at which electrons pass through the cell.

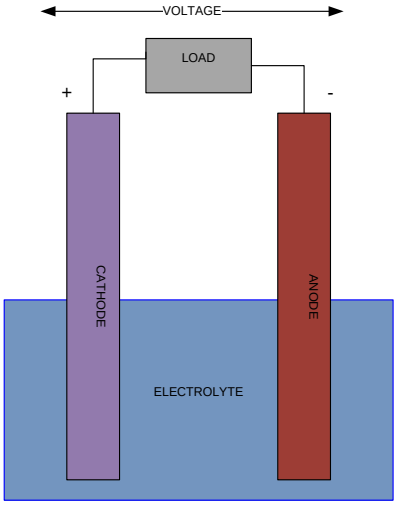

Figure 1 Components of a cell

It is very difficult to achieve a suitable design for a safe, modern, light-weight, high-capacity, high-performance battery. In order to produce a battery with optimized characteristics, the negative electrode, the positive electrode and electrolyte should have some basic features are listed below.

The anode, or negative electrode, supplies electrons to the external circuit and oxidizes at discharge cycle. But during a charging process in secondary batteries, the anode turns into the positive electrode where reduction takes place. For achieving high charge/discharge rates anode must bear high oxidation/reduction rates. Anode should have low electrochemical potential to produce high voltage batteries. Also, to prevent side reactions inside the cell, it should exhibit high columbic efficiency. For high reaction rates, large surface area is another critical parameter for anode material. This can be achieved by using small sized anode active material particles. In some cases, an extra addition of carbon to anode is done to accelerate the reaction. There should be an intimate contact between anode and the electrolyte to achieve efficient electrochemical reactions that can be possible with porous electrode structure. Finally, the anode must not fall apart during the charge/discharge cycle, so a polymeric binder is employed to hold the anode together. All of these requirements listed above are very critical and often conflict with each other. Metals such as Zinc and Lithium are often used as anode materials.

The cathode, or positive electrode, acquires the electrons from the external circuit and reduces at discharge cycle. But during a charging process in secondary batteries, the cathode becomes the negative electrode where oxidation takes place. The requirements for the cathode are the same those for the anode, as explained above. Like anode, the cathode should be stable when in contact with the electrolyte, be environmentally safe and be low cost. Also easy fabrication and long lifetime are other essential criteria that cathode should meet. The materials used for cathode are silver, manganese, metal oxides, and silver chloride.

All of the cathode/anode combinations are not very practical when difficulties in material handling, fabrication and reactivity of the active materials are considered. So, selecting the accurate materials for anode and cathode is an important issue to achieve a successful battery design and meet the expectations for each different application.

The electrolyte provides the ion transfer between the electrodes, so the electrode substance should be ionic conductor. Water solutions of salts, acids, or alkalis, or solid conductors are used as electrolytes in modern batteries. These can be potassium hydroxide, sulfuric acid, organic solvents, zinc oxide, etc.

The separator is used to isolate cathode and anode. If they are not separated, they form short circuit, and the battery discharges. In summary, separator is employed in a battery to avoid contact between the positive and negative electrodes physically in order to prevent internal short circuit. It should be also adequate for the ion transfer between the electrodes and facilitate the current passage and electrolyte movements for electricity generation. Positive and negative plates in a battery can be approximated up to acertain distance due to the internal resistance during charge/discharge operations. The use of separator reduces internal resistance that allows align positive and negative plates next to each other as closer as possible. Separators make possible to design smaller battery systems while reducing the volume. In general, a separator should prevent anode and cathode electrical contact, but also should allow the exchange of ions between to electrodes. The materials for separators are porous plastic, gas fiber separators, or other insulating materials.

2.1.1 Principles of Battery Operation

All electrochemical processes always need the movement of electrons from one chemical to another one by an oxidation-reduction (redox) reaction. So, oxidation-reduction half reactions or redox reactions are the basis of electrochemical cells. While oxidation is the loss of electrons, reduction is the gain of electrons. The oxidation takes place at the "Anode" and the reduction half reaction takes place at the "Cathode". The reaction at the anode releases electrons, and leaves behind positively-charged ions. The reaction at the cathode soaks up electrons. After the reduction reaction the oxidation number decreases, and after the oxidation reactions the oxidation number increases [4-6].

REDUCTION

$$\text{Oxidant} + e^- \longrightarrow \text{Product}$$

(Electrons **gained;** oxidation number **decreases)**

OXIDATION

$$\text{Reductant} \longrightarrow \text{Product} + e^-$$

(Electrons **lost**; oxidation number **increases**)

There are two types of electrochemical cells, Galvanic (Voltaic) Cells and Electrolytic Cells based on redox reactions. In galvanic cells reactions occur spontaneously ($\Delta G < 0$) to generate electrical energy. The system does work on the surroundings. In contrast, nonspontaneous reactions ($\Delta G > 0$) take place in electrolytic cells. So to induce the electrolysis reaction, addition of electrical energy is needed. So, this time the surroundings do the work on the system. Electroplating is the one of the most common applications of electrolytic cell [4, 5].

Batteries produce electrical energy by spontaneous chemical reactions and working principle relies on galvanic cell reaction principle. The chemical energy that is stored in the active materials of both anode and cathode is converted electrical energy by oxidation/reduction reactions. These reactions involve the transfer of electrons and to operate a battery both "oxidation" and "reduction" half reactions should take place [4, 5].

2.1.2 Classification of Batteries – Comparison of Primary and Secondary Batteries

Batteries can be manufactured for single-use or multiple-uses. All batteries are electrochemical cells with a negative electrode, a positive electrode and an electrolyte. Generally, in secondary batteries a separator is also employed to prevent short circuit during the charging process. This charging feature classifies the many different battery systems into two broad categories, "primary batteries" that can be used only for one discharge and "secondary batteries" that can be recharged and used again [7]. Batteries could be recharged, as long as the electrochemical cell reaction is reversible. Consequently, we identify the batteries on their rechargeable property. Batteries are classified as primary (non-rechargeable) and secondary, which have the capability of being recharged by electricity [1].

Primary batteries irreversibly convert the chemical energy into electricity. So the cell reactions of primary batteries are irreversible and active materials cannot be converted to their original form. They put to use the chemicals only for once, for a single discharging process, and then they are thrown away [6, 8].

Secondary Batteries are batteries that chemical reactions can be reversed by passing electricity through the cell in the opposite direction to the current during discharge. This process is called charging. So, charging is a form of electrolytic process involves conversion of the active materials back to their original and reversing the chemical reactions. As a result, secondary batteries are designed for repeated charge/discharge, that is to say cycling processes. Secondary Batteries are also known as "Rechargeable Batteries". It is important to understand that there is also a limit for charge/discharge cycle. Cycling can be done until the capacity of the battery goes down below a practical level and battery becomes out of use. Figure 2 shows that during charging process, oxidation occurs at the cathode; whereas reduction occurs at anode. The reverse takes place during discharging process [9].

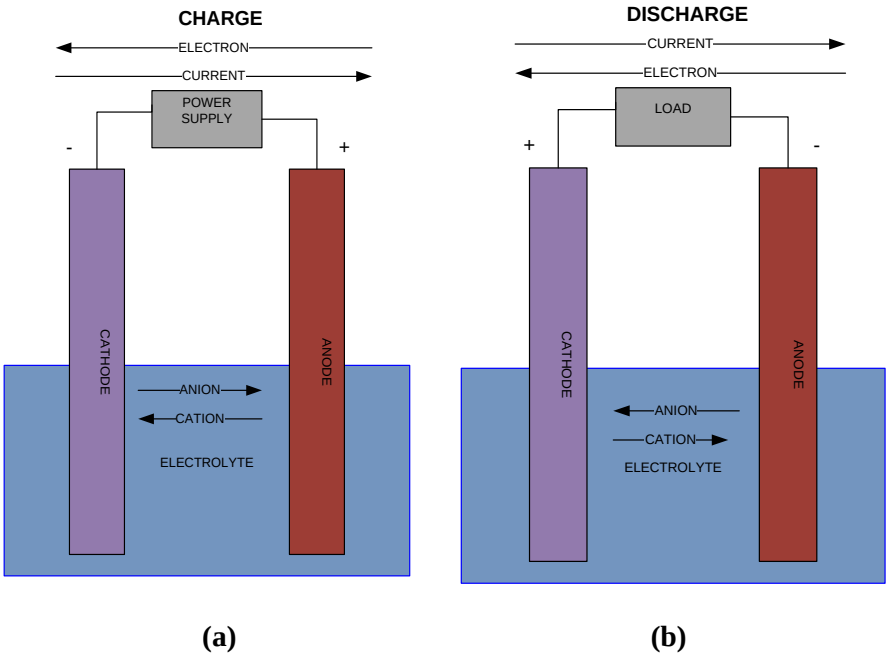

(a) **(b)**

Figure 2 Cell in operation (a) Charging a cell; (b) Discharging a cell

2.2 General Aspects of Divalent Silver Oxide Zinc Battery System

Development studies of silver oxide-zinc batteries date back to 1940s. The first silver oxide-zinc battery is introduced by Michel Yardney and Professor Henri Andre´. Since then silver oxide-zinc batteries are irreplaceable technologies for numerous applications due to their high specific energy and proven safety combination [10]. Even though there are many other battery technologies introduced after silver oxide-zinc battery, this battery still the system of choice where high specific energy/energy density and safety are needed for high-rate, weight or size-sensitive applications [11]. This battery has the highest power output per unit weight and volume of all commercially available batteries. In this battery, silver oxide is used as positive electrode active material and zinc is employed at the negative electrode. Generally, potassium hydroxide is the preferred electrolyte for this system. This chemistry leads to an alkaline battery with high capacity and high voltage characteristics.

The silver oxide-zinc batteries have two versions based on cathode active material. Alternative 1 employs monovalent silver oxide (Ag_2O) whereas alternative 2 employs divalent silver oxide (AgO) as cathode active material. Batteries manufactured by using AgO present 30% additional capacity, which means higher energy density values and nominal voltage, when compared with Ag_2O batteries [12].

2.2.1 Primary Silver Oxide Zinc Batteries

Primary silver oxide-zinc cells are commercially spread as they deliver high energy density and are used in small "button" batteries. They are mainly used in small devices that require constant voltage and long service life. These are watches, calculators, hearing aids, cameras, etc. The application of large sized batteries is limited due to high cost of silver [1]. However, they can be used for high-power applications, for instance launching underwater vehicles, boosters, missiles, torpedoes, and targets [13].

The cell is based on Zn/AgO couple (AgO is the cathode, Zn is the anode) withpotassium hydroxide electrolyte. The nominal voltage of the cell is 1.4 V, the energy density is 160 W-hr/kg, and discharge rate is 10-100 hr (to 0.9 V). They show 200 hr performance at 15 A-hr and operate at temperature range between -40°C and 75°C, and up to 2 years without significant detriment [15]. The impedance is low and uniform. The main characteristics of a primary silver oxide-zinc watch cell by Crompton are listed in Table 1 [14].

Table 1 Performance characteristics of silver oxide-zinc primary watch cells [14]

Energy density		Voltage		Initial nominal rate capacity, mA/cm^2	Life, capacity mA/h per cell	Service years, LCD	Shelf life, years	Temperature °C		Capacity loss per annum at 21°C, %
W-hr/kg	W-hr/l	Nominal	Working					Storage	Operation	
160	680	1.7	1.5	25	52	2.97	5	-40 to 60	-10 to 55	4

2.2.2 Secondary Silver Oxide Zinc Batteries

The secondary silver oxide zinc batteries provide the highest energy per unit of weight among all the commercially available aqueous secondary batteries [1]. The high cost of silver has limited these batteries usages to specific areas. Zinc-silver oxide batteries are used to power and handle high power military devices and weapons. Most military applications need a battery capable of handling high-discharge rates and extended storage life. These batteries have to be fashioned with longevity, high dependability and endurance for challenging environment conditions.

For rechargeable battery-powered military and aerospace systems, zinc-silver oxide batteries have been used because of their high specific energy/energy density, high constant discharge voltage, mechanical ruggedness, and safety. Silver-oxide zinc battery weights 80% less than other batteries generating the same energy. The battery can deliver high capacity at discharge rate of 30 minutes, thus it is used in torpedoes, missile and underwater systems [11]. Due to high density it is popular as energy source for electronic and medical applications, such as satellite and portable equipment [16]. Specially, when used for torpedoes, this zinc- divalent

silver oxide (Zn-AgO) battery systems increases its performance by increasing their speed and range extremely [17].

In this battery chemistry, silver oxide and metallic zinc are used as the positive and negative active materials respectively. Because of the instability of divalent silver oxide (AgO) in alkaline mediums, generally monovalent silver oxide (Ag_2O) is employed as active cathode material [10]. The use of AgO increases the capacity of the battery considerably. Zinc-silver oxide batteries tend to be desirable for high-rate, weight or size-sensitive military applications [18].

The battery requires three types of separators: inner (made of nylon or polypropylene), outer (asbestos and potassium titanate), and primary ion exchange separators (cellophane, fibrous sausage casing). The research for the novel separator materials is a challenge for secondary silver oxide-zinc batteries development [15, 19]. The characteristics of the silver oxide-zinc secondary batteries are summarized in Table 2.

Table 2 Performance characteristics of silver oxide-zinc secondary batteries [20]

Energy density, W-hr/kg	Capacity A/h, per battery	Discharge time	Number of cells	Weight, kg	Cycle life
89	165	0.41	18	100	15

The issue of cycle numbers (higher depth of discharge) depends on zinc in soluble form released to the electrolyte. The electrode changes its shape during the cycles, depending on the discharge and charge rates. The mitigation of this process can be reached by increasing the separator thickness at the plate periphery, while the orientation of the electrode and preparation method do not affect [21].The calcium-containing zinc electrode significantly better performed and provided high capacity, especially over 20 cycles. This is because of calcium zincate complex formation [22, 23]. High concentrations of zincate cause negative plate distortion, and penetration of the separator [20]. The group of Hariprakash proved that the cells with capacities between 10.6 and 58.5 Ah can sustain high-drain applications [24, 25].

2.2.3 Electrochemistry of Divalent Silver Oxide-Zinc System

The electrochemical reactions that take place at silver oxide-zinc batteries are summarized in equation:

$$AgO + Zn + H_2O \leftrightarrow Zn\ OH\ _2 + Ag$$

All the reactions described in this section are reversible. The forward reaction represents discharge process (when the battery generates energy), the beckward reaction shows charge process.

Charge and discharge curves of the silver electrode have two plateaus. The reactions at plateaus at high and low voltage are as follow [26]:

$$2AgO + H_2O + 2e^- \leftrightarrow Ag_2O + 2OH^- \qquad E_0 = 0.607\ V$$
$$Ag_2O + H_2O + 2e^- \leftrightarrow 2Ag + 2OH^- \qquad E_0 = 0.345\ V$$

The reactions above are simplified as in the cell silver (I,III) oxide, namely Ag_4O_4 is formedalong with Ag_2O [27, 28]. At zinc electrode, zinc reacts with hydroxide ion and forms zinc hydroxide:

$$Zn + 2OH^- \leftrightarrow Zn(OH)_2 + 2e^- \qquad E_0 = 1.245\ V$$

The electrochemical reactions have been widely studied. Dirkse and his group studied the overvoltage at silver electrode at range of electrolyte concentration 20-45%. They found rapid anodic overvoltage increase at 30-35% KOH, which is explained by close bound of K^+ and OH^-. Alternatively, they explained it by polarization of Ag+ in a solution [29].

However, the cathodic behavior of zinc includes formation of $Zn(OH)_4$, which then dissolves and forms $Zn(OH)_2$ [18]. The electrode passivation by zincate formation on the electrode surface is a challenge for process improvement. The changes of zinc electrode during the reaction have been reviewed in the work of Poa and Wu [30]. They added a layer of non-woven fabric treated with Fe_2O_3 to the edge sections of the separator. This allowed suppressing the zinc electrode shape change [31]. A review by Gainereports that hydrophilic and hydrophobic additives are capable of stabilizing the electrode structure; surfactants are proved to control dendrite and growth and prevent zinc agglomeration [10]. The invention offers cadmium additive to zinc electrode for improvement of surface morphology to retain zinc reduced from the solid compound [32]. Also another method for modifying the electrode with nickel, copper, silver and bismuth oxide was developed by Casey and Serenyi [33, 34].

2.2.4 Advantages and Disadvantages of Silver Oxide-Zinc Batteries

Advantages

The zinc silver oxide batteries discharge at flat, constant voltage at both high and low-current rates. Secondary batteries provide high currents, high capacity, theoretically up to 440 W-hr/kg (for example, lead-acid battery provides 30 W-hr/kg) [14, 35]. The battery shows 95% of its initial capacity after a year of storage at room temperature, they are able to operate at wide temperature range, between -40°C and 73°C. When their good dry shelf life and wide operation temperature characteristics considered with their excellent electrochemical efficiency, they become key energy sources for military applications. They prove moderate shelf life (Eagle Picher claims a dry shelf life of 2.5 years, and wet shelf life of 1 year). The capacities of the cells can be between 0.1 A-hr to 20 000 A-hr. The leakage and salting of the battery are negligible; batteries are not shock and vibration sensible [1]. All of these advantages make silver oxide-zinc batteries desirable when compared with other rechargeable battery technologies.

Disadvantages

The secondary batteries typically have limited depth of discharge, and silver oxide often has dual voltage discharge curves and high instability in alkaline solutions [36].The batteries suffer from short cycle life due to zinc mass redistribution, changes in zinc morphology [15].

Silver oxide electrodes have been reported as instable. This causes the capacity loss and delayed activation in reserve batteries. The instability is caused by metal contaminants that destabilize the oxide. As a result, the lower capacity monovalent oxide is formed. The authors propose chemical preparation of AgO to minimize the electrode aging [36].

2.3 Silver Oxide

Silver oxide is a leading source for developing high power silver oxide-zinc batteries. Divalent silver oxide (AgO) and monovalent silver oxide (Ag_2O) are the two types of silver oxides employed as cathode material. Silver oxide-zinc batteries that are produced with AgO in cathodes tend to have higher theoretical voltage (1.80 V), higher energy density (424 Wh/kg), higher conductivity and lower specific resistance in comparison to Ag_2O cathode employed silver oxide-zinc batteries [18]. This higher energy density of AgO results in production of higher electricity per mole. Thus, weight and space saving is possible due to lower silver oxide consumption. With respect to these advantages, AgO is the first choice of silver oxide-zinc battery producers as the main cathode component [37].

Table 3 A comparison of chemical properties of AgO and Ag_2O [18]

Chemical Properties	**AgO**	**Ag_2O**
Atomic or Molecular Weight (g)	123.8	231.7
Density(g/cm^3)	7.4	7.1
Theoretical Potential (V)	1.80	1.60
Theoretical Capacity (Ah/g)	0.432	0.231
Gravimetric Energy Density (Wh/kg)	424	370

AgO is an inorganic semiconductor and diamagnetic grayish black chemical in powder form with monoclinic crystal structure. It has a theoretical silver content of 87.08% plus 12.92 % theoretical oxygen content. The most common method for preparation of AgO is the oxidation of silver nitrate with potassium persulfate in strong alkaline solutions [38]. It has an unusual structure with more than one oxidation state [39]. Although, the empirical formula of AgO caused to think it is in +2 oxidation state, actually it is a mixed valance compound and formulated as $Ag^{I}Ag^{III}O_2$ or $Ag_2O.Ag_2O_3$ [39, 40].

Table 4 Properties of divalent silver oxide [41]

IUPAC Name	Silver (I,III) Oxide
Other Names	Silver Peroxide, Argentic Oxide, Silver Suboxide
CAS Number	1301-96-8
Properties	
Molecular Formula	AgO $Ag_2O.Ag_2O_3$
Molar Mass	123.87 g/mol
Appearance	grey-black powder diamagnetic
Density	7.48 g/cm^3
Melting Point	>100 °C, decomposition
Solubility in Water	0.0027 g/100 mL
Solubility	Soluble in alkalis

2.3.1 Nanosized Silver Oxide

2.3.1.1 Application Areas

The unique physiochemical properties of the nanoparticles combined with the growth inhibitory capacity against microbes has led to the upsurge in the research on nanoparticles and their potential application as antimicrobials. From centuries metals such as silver have been used for treating burns and chronic wounds, and copper has been used to make water potable. It is quite evident that some of the metallic compounds possess antimicrobial property.

Recently, the confluence of nanotechnology and biology has brought to fore metals in the form of nanoparticles as potential antimicrobial agents. Nanoparticles have unique and well defined physical and chemical properties which can be manipulated suitably for desired applications. Moreover, their potent antimicrobial efficiency due to the large surface area to volume ratio has provided them an edge over their chemical counterparts which are facing the problems of drug resistance.

Silver compounds have been used to treat burns, wounds and infections [42]. Various salts of silver and their derivatives are used as antimicrobial agents [43, 44]. Recent studies have reported that nanosized silver oxide particles exhibit antimicrobial properties [45, 46]. Nanoparticles of silver oxide have been studied as a medium for antibiotic delivery, and to synthesize composites for use as disinfecting filters and coating materials [47, 48]. It is assumed that the high affinity of silver towards sulfur and phosphorus is the key element of

the antimicrobial effects. Metal oxide nanoparticles with antimicrobial activity when embedded and coated on to surfaces can find immense applications in water treatment, synthetic textiles, biomedical and surgical devices, food processing and packaging [49].

The silver oxide nanoparticles can be applied as microelectronic and bacteriostatic, catalytic or magnetic recording materials. Also, silver oxide nanoparticles can be used as antistatic, cryogenic or superconducting materials [50, 51].

2.3.1.2 Physical and Chemical Properties

The materials have their properties defined by the chemical composition and the microstructure presented on them. The quantification of crystalline phases is a key step in determining the structure, properties and applications of a given material. Therefore, the study of the amount of crystalline phases present in a material represents an important parameter to control the microstructure and the correlation of the properties associated with the developed stage in the process. The distribution of phases or microstructure depends on the manufacturing techniques, raw materials used, equilibrium reactions, kinetics and phase changes. The characterization of crystalline microstructure, regarding the density, atomic distribution and unit cell dimensions, contributes to the control of the manufacturing process. In Table 5, we have summarized the crystal structure data of AgO, Ag_2O, HT-Ag_2CO_3 and RT-Ag_2CO_3. Within this study, determination of crystalline phases in produced powders using the technique of X-ray diffraction was performed by the data presented in Table 5.

The nanoparticles, as any colloidal particles, are characterized by size (1-1000 nm), form (cubes, pyramids, triangular plates) and surface tension [52]. Their properties differ depending on their size. The nanoparticles possess novel properties that differ from the bulk material. The divalent silver oxide that is produced by chemical precipitation methods is stable in alkaline solution and slow in spread of oxygen generation. It is low cost for batteries production with high energy density [12, 53].

In his work Smith mentions that chemically prepared silver oxide electrodes provide better performance, namely high efficiency rates (500 mA/cm^2), low polarization and provide higher energy density [54]. The research group lead by Liu found that if the active material has 10-35% admixture of nanosized silver oxide, it improves the periodic charge–discharge performance [55].

Table 5 Crystal structure data of AgO, Ag_2O, HT-Ag_2CO_3 and T-Ag_2CO_3

	AgO				**Ag_2O**				
General									
Origin	ICSD				ICSD				
Code	43741				31058				
Phase Data									
Space-Group	P 1 21/c 1 (14)				P n -3 m (224)				
Cell Parameters	a=5.8520 Å b=3.4780 Å c=5.4950 Å β=107.5000°				a=4.7180 Å				
Atomic Parameters									
Atom	**Wyck.**	**x/a**	**y/b**	**z/c**	**Atom**	**Wyck.**	**x/a**	**y/b**	**z/c**
Ag1	2a	0	0	0	Ag1	4b	1/4	1/4	1/4
Ag2	2d	1/2	0	1/2	O1	2a	0	0	0
O1	4e	0.29500	0.35000	0.23000					

	HT-Ag_2CO_3				**RT-Ag_2CO_3**				
General									
Origin	Pearson				ICSD				
Code	1905229				8011				
Phase Data									
Space-Group	P 3 1 c (159)				P 1 21/m 1 (11)				
Cell Parameters	a=9.1716 Å c=6.5176 Å				a=4.852(4) Å b=9.553(8) Å c=3.255(4) Å β=91.9600°				
Atomic Parameters									
Atom	**Wyck.**	**x/a**	**y/b**	**z/c**	**Atom**	**Wyck.**	**x/a**	**y/b**	**z/c**
Ag1	6c	0.01570	0.33360	0.39300	Ag1	4f	0.2109(2)	0.0781(1)	0.2191(2)
O1	6c	0.06650	0.15640	0.00000	O1	2e	-0.018(2)	1/4	0.889(3)
O2	6c	0.25260	0.50970	0.17680	O2	4f	0.390(1)	0.6342(7)	0.334(2)
Ag2	6c	0.35430	0.32520	0.14010	C1	2e	0.270(3)	3/4	0.261(4)
O3	6c	0.56220	0.17960	0.16510					
C2	2b	1/3	2/3	0.17680					
C3	2b	1/3	2/3	0.66510					
C1	2a	0	0	0					

2.3.2 Production Methods of Nanosized Divalent Silver Oxide

2.3.2.1 Electrochemical Precipitation

The electrochemical preparation method involves electrochemical oxidation of silver metal in alkaline solutions. Generally, electrochemical precipitation of nano sized silver is performed by using $AgClO_4$, $AgBF_4$, and $AgPF_6$. The substances are oxidized anodically at pH 6-7, average temperature of 0˚C, and average current of 200 A/m^2 [56]. The method requires a protecting agent such as zeolite, polyvinyl pyrrolidone, or polyphenylpyrrole. Nanospheroid particles of 1-20 nm can be obtained by electrochemical precipitation methods [51]. It is a lengthy, complicated and relatively expensive approach for synthesizing divalent silver oxide nanoparticles. Also it is a high cost procedure and results with low purity. Product has a non-uniform stoichiometry (Ag_2O/AgO mixture); therefore time consuming

purification steps are required. The advantage of the electrochemical method is the possibility of large-scale realization [57].

The electrochemical laser-based method for silver oxide formation is described by Yan [58]. It allows producing particles with well-defined morphology (cubes, pyramids, triangular plates). The stabilizing agent was Polysorbate 80, as well as other surfactants.

2.3.2.2 Chemical Precipitation

The nano-sized silver oxide can be formed by conducting a neutralization reaction. A strong base that serves as a neutralization medium is prepared by using one or both of sodium or potassium hydroxides [59]. Adding the silver salt solution simultaneously to this aqueous solution initiates a neutralization reaction. In his work Harigae et al. prepared a neutralization medium by adding silver salt to sodium/potassium hydroxide solution, and obtained nano sized silver oxide particles. The average primary particle diameter is estimated as 1-50 nm and the average secondary particle diameter is estimated as 1-1000nm [60].

Also, the surface of nano-sized silver oxide can be coated with a thin layer of surfactant (fatty acid, dodecyl sulphate, polyvinyl pyrrolidone) which encapsulates (stabilizes) the nanoparticles from aggregation [61, 62]. The surfactants also allow reducing the concentration of silver solution needed for precipitation [63]. The detailed procedure for the process is described by Berube [64, 65].The procedure for producing silver oxide nano particles sized 2-10 mm, developed in Hussain patent [66]. When thermal treatment is applied, a silver layer is produced on silver oxide nano particles [67].The size-controlled chemical synthesis of nano particles is reported by Evanoff et al. [68].

2.3.2.2.1 Sonocrystallization

Sonocrystallization is the application of high intensity, low frequency ultrasound to a reaction that allows complete control on crystallization. It allows extremely accurate control of nucleation, a process which is random and very difficult to control by conventional techniques.

The following advantages can be observed in sonocrystallization applied chemical reactions [84]:

- Increase in reaction speed
- Increase in reaction output
- More efficient energy usage
- Performance improvement of phase transfer catalysts
- Activation of metals and solids
- Increase in the reactivity of reagents or catalysts
- Improvement of particle synthesis

This acoustic cavitation results in a sophisticated control of process parameters. Lyczko et al. reported a decrease of induction time after sonocrystallization [85]. An increase in nucleation rate is reported by another study [86]. Also, increase in reproducibility, decrease in crystal growth rate and particle size and various effects on crystal shape and characteristics are

reported effects of sonocrystallization in literature [86-88]. The mechanism responsible for these effects is still unknown, although several have been proposed. The use of ultrasound in the synthesis of metal oxides, for example, has some promise as well.

A myriad of metal oxides have been prepared by sonochemical techniques. Gedanken and coworkers have reported various nanostructured metal oxide syntheses including TiO_2,Fe_3O_4, a-$Ni(OH)_2$, GaO(OH), $In(OH)_3$ and $BaFe_{12}O_{19}$[76, 89-93]. In their syntheses, sonication of an aqueous metal salt solution is carried out under ambient conditions (usually in the presence of air) to prepare various forms of nanostructured metal oxides. For instance, nanometer-sized a-nickel hydroxide was prepared simply by sonicating an aqueous solution of nickel nitrate and urea [91]. It is believed that ultrasonic irradiation significantly enhances the hydrolysis rate, and shock waves can induce unusual morphological changes in metal oxides.

The advantages of the sonochemical approach over conventional methods in the synthesis of metal oxides, including more uniform size distribution, a higher surface area, faster reaction time, and improved phase purity, have been recognized by many research groups. Examples of successful sonochemical syntheses include TiO2, ZnO, CeO_2, V_2O_5, In_2O_3, $ZnFe_2O_4$, $PbWO_4$, $BiPO_4$, and $ZnAl_2O_4$ [56, 94-105]. Yu and coworkers revealed that sonochemically prepared titania nanoparticles are more photocatalytically active than commercial titania nanoparticles. Such enhancement was attributed to improved crystallinity of titania caused by a faster hydrolysis rate in the presence of ultrasound.

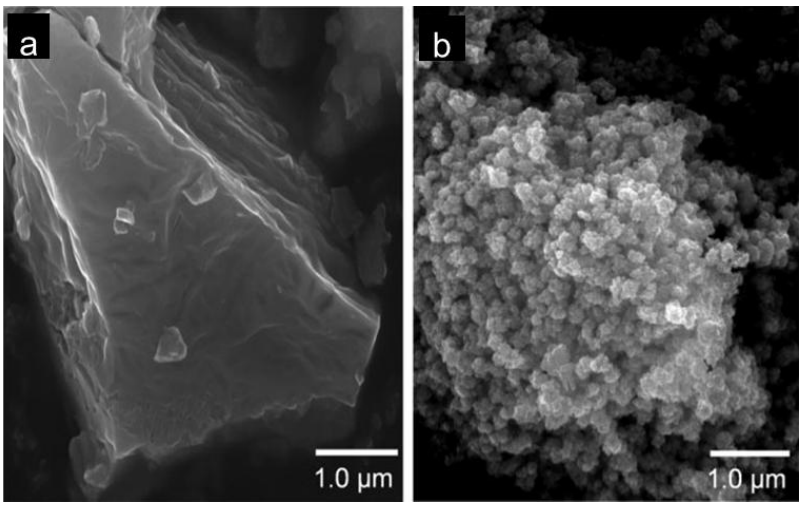

Figure 3 SEM Images of (a) conventionally and (b) sonochemically prepared MoS_2[106].

2.3.2.3 Characterization of Nano Silver Oxide

The nanosized AgO particles are characterized by various techniques used in material science [69]. Some of those methods are transmission and scanning electron microscopy, X-

Ray diffraction, neutron diffraction, FTIR, ultra-violet absorption, thermogravimetry, gas chromatography, BET surface area measurements and so on [37, 70-72].

The work of Mansour summarizes the results of the structural investigations and proposes to use structural investigation to study changes in chemical composition of silver oxide cathode during the storage [73].

CHAPTER 3

EXPERIMENTAL

This chapter outlines the experimental procedures, equipment, and material characterization techniques used in the current research, in the chemical preparation of high purity nano divalent silver oxide with high speed charge/discharge ability, for application as cathode active material for AgO-Zn battery. The effect of the synthesis parameters on the final AgO powder was investigated. The AgO powder was characterized during/after precipitation reaction to evaluate the various AgO properties, such as, phase identification and purity, particle size, and structure.

The reported manufacturing procedure used to prepare AgO nanopowder in the first stage of this study was based on the chemical precipitation process by oxidation of alkaline $AgNO_3$ on a laboratory scaled version. The properties obtained from the other powders produced in literature and the current research results were examined and compared with each other to identify the factors affecting the final properties yielded. The observations aided in the optimization of the process parameters for chemical precipitation at the powder production stage. These collected data are used in the investigation of surfactant effect and sonocrystallization process on particle size in chemical precipitation method.

Three experimental designs were constructed: (i) Reaction development and process screening by using a computer-controlled, jacketed vessel reactor system that can monitor, and control process parameters such as temperature, pH, turbidity, and stirrer speed and reagent addition. (ii) Reaction optimization by screening the factors and optimizing the critical parameters which have a significant effect on the powder properties. This is followed by shape and size control of the silver oxide by changing the amount of surfactant present in the reaction mixture (iii) Understanding the effect of the sonocrystallization on morphology, structure and size of the particles.

All experimental designs and approaches, including reactor system, test set up, and characterization instruments, used in the research are outlined in following sections.

3.1 Materials

Silver nitrate ($AgNO_3$, 99.5%) was purchased from Ardan Chemicals and research grade sodium hydroxide (NaOH, 99%), potassium persulfate ($K_2S_2O_8$, 99%), and CMC (Carboxymethyl cellulose, M_w 1000) were purchased from KIMETSAN. CTAB (Cetyl trimethylammonium bromide), SDBS (Sodium dodecylbenzenesulfonate), PEG 400 (polyethylene glycol 400), and IGEPALCA-630 (octylphenoxypolyethoxyethanol) were purchased from Sigma-Aldrich. All chemicals were used without further purification. Ultra pure water (18.2 MΩ.cm@25°C) was used throughout all experiments.

3.2 Methods and Experimental Set-Up

An oxidation solution was prepared by dissolving 12.75 gr $AgNO_3$ in 0.05 lt ultrapure water. Separately, a reducing solution was prepared by dissolving 10.80 gr NaOH and 10.95 gr $K_2S_2O_8$ in 0.25 lt ultrapure water together. The resulted reducing solution was heated while stirring. AgO particles were produced by dropping $AgNO_3$ solution into the NaOH-$K_2S_2O_8$ solution with the help of a syringe pump. After all solutions were added, the mixed solution was stirred further. The precipitated AgO particles were separated and collected by centrifuge. Then, the product was dried under vacuum. The chemical precipitation reaction explained above can be represented by the equation shown below;

$$4AgNO_3 + 2K_2S_20_8 + 8NaOH \rightarrow 4AgO + K_2S0_4 + 2NaHO_3 + 2KNO_3 + 4H_2O$$

The experiments were carried out in a one liter jacketed vessel reactor. Also, for sonocrystallization experiments a sonochemical system was used. Both systems were purchased from Syrris. The temperature is controlled in every experiment with controlling heating/cooling from circulator, and the reactor system was also equipped with a stirrer (Figure 4).

Figure 4 Experimental Set-Up

The parameters that were varied to produce the particles in the desired size, structure and shape studied in this research are : i) reaction temperature: 40 $^{\circ}$C, 60 $^{\circ}$C, 80 $^{\circ}$C, ii) $AgNO_3$ addition rate: 10 ml/min, 20 ml/min, 100 ml/min, iii) $[K_2S_2O_8]$/[NaOH] mole ratio: 0.1, 0.12, 0.15, 0.18, iv) concentration of surfactant molecules: 0.01 % to 1.0 % wt. of IGEPAL CA-630, PEG 400, CTAB, SDBS and CMC, v) sonocrystallization: pulsed sonication 10, 20, 30, 40, 50, and 60 W. Throughout the parametric study, only one parameter was changed, while the others were kept constant.

3.3 Characterization Methods

The AgO powders were structurally characterized by using scanning electron microscopy (SEM), X-Ray diffraction (XRD), and particle size analyzer.

Scanning electron microscopy (SEM) studies were acquired using FEI Nova Nano SEM 430 microscope. In the preparation step, the powder samples were mounted onto double-stick tape. Because AgO is conductive, no surface coating was necessary before the insertion into the chamber.

Particle size analysis and the particle size distribution of the divalent silver oxide were performed in this research using Malvern Mastersizer 2000. Wet and dry measurement modes are available in this characterization instrument. Because silver oxide has a tendency to agglomerate when dry, it is used in wet measurement mode. A representative amount of sample was introduced into the equipment during all measurements.

X-Ray studies were performed with a Rigaku D/Max-2000 pc diffractometer (Cu Kα, λ = 1.5406 Å, 40 kV and 100 mA, graphite monochromator, scintillator detector, step scanning 1 °/min). For crystal structure measurements and phase determination, the instrument scans a given range of angles between the X-ray source, the sample and the detector automatically. In this thesis work, scans are run between 10° to 90°. The Rietveld method is used to refine the crystal structure model of a material. It can be used for quantitative phase ID, lattice parameter and crystallite size calculations, and determine atom positions and occupancies.

CHAPTER 4

RESULTS AND DISCUSSION

In this thesis, AgO nanoparticles were synthesized through chemical precipitation method. This method, which is adapted from the work of Murakami et al [53], is modified to decrease particle size and reach uniform particle size distribution. Chemical precipitation of AgO, using different surfactant chemistries is studied. The use of surfactant stabilizes the particle, slows down the growth rate, and as a result particle with smaller median particle size can be obtained. Since firstly used by Hoar and Schulman [74] in 1943 as surfactant, CTAB was investigated thoroughly for the synthesis of nanoparticles [75]. CTAB was used as growth controlling agent for production of AgO nanoparticles. Also, the effect of anionic surfactants on AgO particle size was studied by running experiments in the presence of SDBS and CMC. Other used surfactants in this study were both nonionic, PEG 400 and IGEPAL CA-630.

The use of ultrasound in the synthesis of metal oxides has some promise as well [76]. In the past, some successful attempts have been made to synthesize the nanoparticles of metal oxides by chemical methods [77-80]. Recently, sonochemical processing has been proven as a useful technique for generating novel materials with unusual properties. Sonochemistry arises from acoustic cavitation phenomenon, that is, the formation, growth and implosive collapse of bubbles in a liquid medium [81]. Therefore, sonocrystallization allows extremely accurate control of nucleation, a process which is random and very difficult to control by conventional techniques. Based on these studies, the effect of sonocrystallization on AgO nanoparticles' size and morphology were also studied in this research.

Control over chemical reaction parameters such as temperature of the reaction, addition rate, molar ratio and concentration of the reactants were also studied. It was observed that these parameters played crucial roles on the morphology, yield and structural purity of the materials produced.

4.1 Determination of the Chemical Precipitation Process Parameters

The Rietveld method is used to refine the crystal structure model of a material. Rietveld Method, which is based on the simulation of the diffraction profile from the structures of the

phase components in a sample, allows more information to be extracted from the XRD patterns. Analyzing the entire diffraction pattern and using the intensities of each individual angular step, the method enabled the refinement of complex crystal structures with the choice of a theoretical model of the structure through a database, and subsequent entry of the theoretical data in the program, followed by the step of refining the experimental parameters. The variables contain in the input the data necessary for the construction of the calculated diffraction pattern, ie, data on the crystal structure of the material. The main data are: 2θ limits, wavelengths of radiation used, specification of the background radiation, the space group symbol, symbol and valence of each atom (used for entering tables scattering factors) and number of phases.

The quality of refinement is verified by numerical statistical indicators. The residue R_W considers the error associated with each intensity value by the number of counts, using the weighting factor w (2θ). The value of R_W for good results is 2-10%, while the typical values obtained range from 10-20%. R_W is related to the quality of the experimental diffractogram, this value being smaller is better. In practice, differences of up to 20% between REXP and RP are acceptable. The factors that modify the R_W are differences in the peaks (as the width) and the background radiation.

The Figure 5 shows the X-ray diffractogram of AgO synthesized at 40 °C with varying reaction times. The presented crystalline phases were identified using the JCPDS and ICSD database. In order to estimate the relative amount of each crystalline phase, the XRD experimental spectrum was simulated using the Rietveld method for structure refinement. Crystallographic data (atomic coordinates, space group, cell parameters and temperature factor) used were those presented in Table 6. These are the input information for the refinement, which consists in comparing the structure of theoretical models and the observed spectrum. The described procedure is applied to all samples and the detailed phase analysis results are given in the following sections.

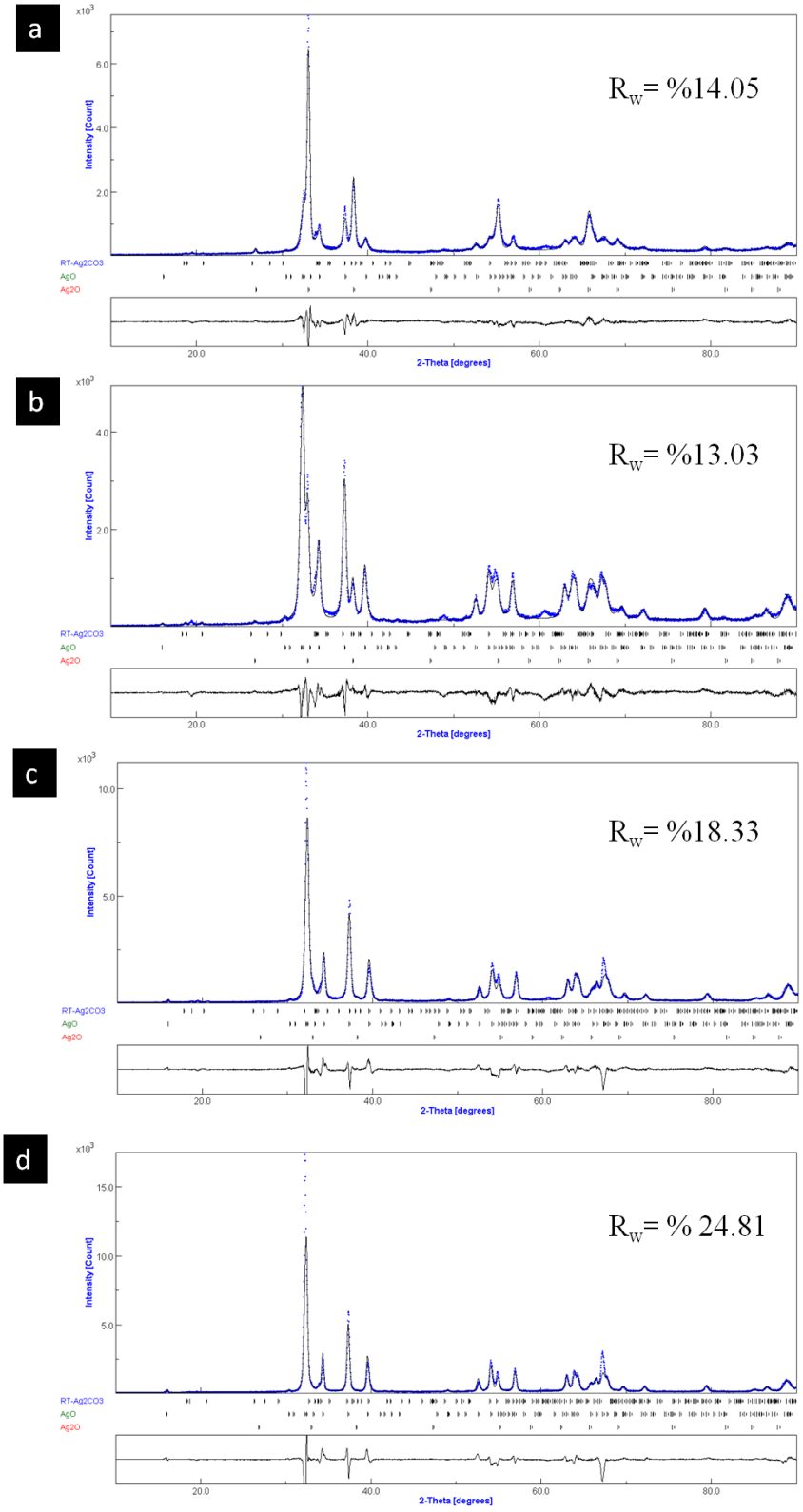

Figure 5 XRD patterns of AgO: experimental (black lines) and simulated by the Rietveld Method (blue lines): at reaction temperature of 40 °C and reaction times (a) 70 min, (b) 140 min, (c) 210 min, and (d) 280 min.

4.1.1 Dependence of the Reaction on Temperature

Temperature is one of the key influence factors in chemical precipitation reactions. It affects the kinetics of the product formation and thermodynamic stability of the final product. In crystallization kinetics, two stages are involved, a short burst of nucleation occurs when the concentration of the species reaches critical supersaturation, and then, there is a slow growth of the nuclei by diffusion of the solutes to the surface of the crystal. The degree of supersaturation controls whether the reaction is nucleation or growth controlled. So, the control of the nucleation and growth process by supersaturation of the solution is the key to direct the particle size. To produce mono disperse AgO nanoparticles, these two stages should be separated; i.e, nucleation should be avoided during the period of growth. Size control of mono dispersed particles must normally be performed during the very short nucleation period, because the final particle number is determined by the end of the nucleation and it does not change during particle growth. Temperature often influences nucleation and crystal growth by manipulating the solubility and supersaturation of the sample. Increasing temperature will increase or decrease the solubility of the species in solution, hence increasing or decreasing the supersaturation. In order to investigate the influence of reaction temperature in the synthesis of silver oxide particles, several experiments were carried out. The first set was related to the reaction temperature. Experiments were carried out 40, 60, and 80 °C respectively and all other reaction parameters were kept constant.

Altering of these kinetic and thermodynamic factors by temperature can lead to the formation of desired crystals in precipitation chemistry. In this study, it has been observed that change in reaction temperatures influenced the morphology, structural purity, uniformity and particle size distribution of the synthesized nanoparticles. SEM images of AgO particles synthesized at temperatures of 40, 60, and 80 °C are shown in Figure 6(a)-(c), respectively. Although, AgO particle synthesis was observed at all studied temperature, shape and size of the particles vary with temperature critically. The change in the particle size of AgO with temperature was illustrated at a plot provided in Figure 6 (d). At 40 °C, non-uniform particles with very high particle sizes started to form (Figure 6(a)). Also particle size distribution was very broad at 40 °C; changing from 1.035 µm to 12.368 µm. Low rate of crystal growth along with a high supersaturation at this temperature were most likely the reasons for the unwanted crystal growth. Size of the particles decrease, and size distribution become narrower between 40-60 °C. The smallest diameter and particle distribution range were obtained when the reaction was carried out at 60 °C. Increasing the temperature to 80°C, results in increase both of particle size and distribution as shown in Figure 6 (e). This is most likely due to the disruption of dissolution–crystallization dynamic equilibrium through high dissolution rate at this temperature. This suggests that the optimum degree of supersaturation and dynamic equilibrium were reached at 60 °C for the synthesis of AgO particles with desired properties. Further increase of temperature increases the dissolution rate and thus disturbs the equilibrium between dissolution and crystallization processes. The silver oxide precipitation reaction is found to be exothermic and increasing the temperature of exothermic reactions will accelerate in the favor of reactants. Figure 6 (f) shows the behavior of the system to an increase in the reaction temperature. When the temperature is between 40-60 °C, the rate of conversion was increased. However, increasing temperature further, decreases the yield of the product. This might accelerate the reaction to proceed in the reverse direction and remove the added heat, by converting products back to reactants. Thus, the conversion rate went down and the shift of the equilibrium in favor of crystallization resulted in unwanted increase of particle diameter.

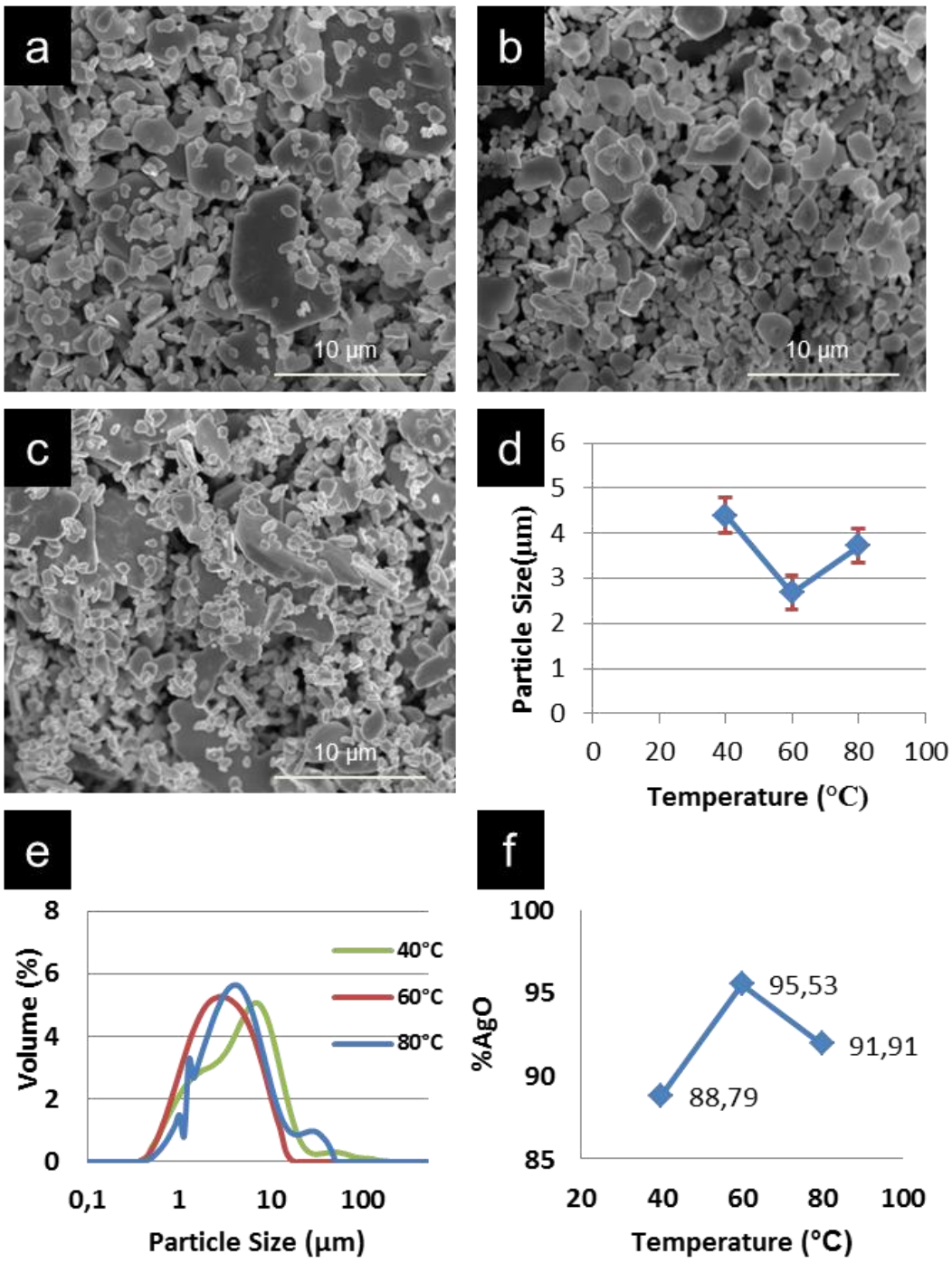

Figure 6 SEM Images of AgO particles synthesized at different temperatures (a) 40, (b) 60, (c) 80 °C. (d) Changes in particle diameter with reaction temperature. (e) Particle size distribution of AgO particles synthesized at different temperatures. (f) Effect of reaction temperature on % AgO yield. ($[K_2S_2O_8]$/[NaOH] Mole Ratio: 0.18; Mixing Speed: 500 rpm; $AgNO_3$ Solution Addition Rate: 100 ml/min).

4.1.2 Dependence of the Reaction on Time

The particle size and distribution of the AgO can be regulated by the control of reaction time. Reaction time is found to affect predominantly the resultant AgO by means of crystalline phase fraction, crystalline size and, thus, specific surface area. By controlling the reaction time, Y. Sun et al. varied the structural purity and morphology during the production of silver nano-particles [82]. It is clear from this study that precise control of reaction time with simultaneous optimization can prevent disruption of nano particle morphology. A pure-phase AgO with high yield, desired morphology, and morphological purity could therefore be prepared by adjusting the reaction time.

The reaction time effect was investigated at 40, 60 and 80 ºC for 280 min, 150 min, and 40 min respectively. Figure 7 demonstrates the temperature-reaction completion time relation and the effect of reaction time on the product yield. In order to estimate reaction completion time, samples were withdrawn from the reactor during the experiment in equal time intervals to assess the AgO content and the presence of different phases in the samples. The point at which AgO % vol. reaches maximum, accepted as reaction completion point. The samples were examined by XRD, and Figure 7 (a), (b) and (c) are generated from the XRD data created by Rietveld method. Figure 7 (a) shows the XRD results of AgO samples at reaction times 70 min, 140 min, 210 min, and 280 min at 40 °C reaction temperature. At 70 min, the purity of the product was very low because of the high by-product formation percentage. When time was prolonged, AgO formation increased and the maximum AgO wt. % was reached at 210 min for 40 °C reaction temperature. However, particle size distribution is very broad at 40 °C and purity of product was still low. The effect of reaction time on particle size was also investigated at 60 °C and in the range of 40 min-150 min, while maintaining the other parameters constant. After 120 minutes, amount of reaction intermediate started to increase. This is mainly the result of exothermic reaction characteristics. As the reaction time is prolonged, the system reacted to remove the added heat, thus the reaction proceeded in the reverse direction, converting resultant AgO back to half product Ag_2O. The continuous fall of percentage of the weight of other by-products HT-Ag_2CO_3 and RT-Ag_2CO_3, supports the aforementioned situation. Highest AgO wt. % is observed when reaction was terminated at 120 min (Figure 7(b)) among all other studied temperature and time values. Further extension of reaction time results in low purity particles. Figure 7 (c) shows the XRD results of AgO samples at reaction times 10 min, 20 min, 30 min, and 40 min at 80 °C reaction temperature. The optimum reaction time is found to be 30 min and increasing the reaction time to 40 min, results in decrease of AgO wt. %.

As a result, the optimum time was determined as 120 min for the reactions carried out at 60 °C (Figure 7 (d)-(e)). Murakami et al. reported the optimum synthesizing time for the production of AgO as 100 min at 60 °C [83], based on the relation between the reaction time and gas generating rate. It is to be noted, however, that such AgO formation time can be established only in certain limited conditions, and may be varied, for example, with variation of the stirring speed or other factors.

a

Experiment		Ag_2O	AgO	HT-Ag_2O_3	RT-Ag_2O_3
T(°C)	Reaction Time (min)	Wt. %	Wt. %	Wt. %	Wt. %
40	70	61.38	27.58	2.24	8.78
	140	18.73	68.68	6.24	6.34
	210	4.38	88.79	1.69	5.12
	280	12.37	72.1	1.12	13.58

b

Experiment		Ag_2O	AgO	HT-Ag_2O_3	RT-Ag_2O_3
T(°C)	Reaction Time (min)	Wt. %	Wt. %	Wt. %	Wt. %
60	40	29.56	46.72	2.8	20.91
	80	6.53	86.85	1.85	4.76
	120	1.39	95.53	1.58	1.48
	150	3.9	93.79	1.25	1.05

c

Experiment		Ag_2O	AgO	HT-Ag_2O_3	RT-Ag_2O_3
T(°C)	Reaction Time (min)	Wt. %	Wt. %	Wt. %	Wt. %
80	10	29.04	67.59	1.47	1.88
	20	7.88	86.07	2.49	3.54
	30	5.11	91.91	2.78	0.19
	40	8.12	89.06	1.92	0.9

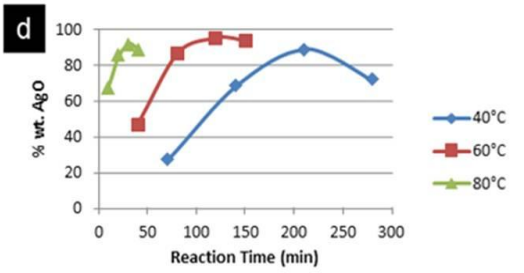

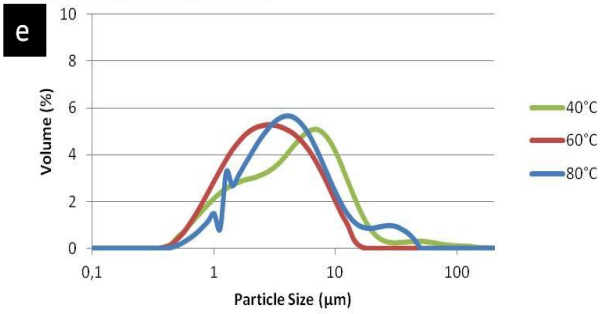

Figure 7 Effect of reaction time on the product yield (a) 40, (b) 60, (c) 80 °C. (d) Comparison of reaction completion times at different temperatures ($[K_2S_2O_8]/[NaOH]$ Mole Ratio: 0.18, Mixing Speed: 500 rpm, $AgNO_3$ Feed Rate: 100 ml/min). (e) Size distribution of AgO particles synthesized at different temperatures. ($[K_2S_2O_8]/[NaOH]$ Mole Ratio: 0.18, Mixing Speed: 500 rpm, $AgNO_3$ Feed Rate: 100 ml/min).

4.1.3 Effect of AgNO3 Addition Rate on Particle Size

A semi-batch process is created by feeding silver salt ($AgNO_3$) into the jacketed vessel reactor at a constant feed rate that contains other reactants ($K_2S_2O_8$/NaOH) previously. Running the reaction under a semi-batch process gives us the opportunity to have a better control over particle size, morphology and shape than batch systems. We can easily control the concentration or moles of the reactants which helps us to improve selectivity of the reaction. Also, greater control of the heat production and temperature of the precipitation reaction is possible. Because, reaction proceeds as reactants are added, it is easier to fix the temperature at a certain value and keeping heat production rate slow.

Figure 8 presents the effect of addition rate of the silver salt on particle size distribution. The changes in particle size distribution with different addition rates are shown in Figure 8. When the reaction was run for 10 ml/min addition rate of $AgNO_3$, non-uniform particles with very high particle sizes started to form (Figure 8 (a)). Significant decrease in size of particles was observed as the addition rate decreased to 20 ml/min (Figure 8 (b)). At this addition rate, still some big crystals with different morphologies were formed. As the feed rate was increased further, particle size was decreased with a uniform crystal structure (Figure 8 (c)). Larger AgO particles disappeared and smaller, more uniform and faceted particles were formed. It is known that the addition rate has a significant effect on residence time. At higher addition rates, the residence time becomes shorter, so the particles cannot grow and aggregate, and the particle size decreases. By this way, we can obtain nuclei with the same size and shape, because they are produced under the same experimental conditions. As a result, monosized AgO can be synthesized by maintaining the residence time as short as possible.

Also, Figure 8 (c) shows particle size and feed rate relation in detail. As the $AgNO_3$ addition rate increased, the particle size decreases significantly. The median particle size decreases 3.836 to 2.426 μm with increasing the addition rate from 10 to 100 ml/min. Thus, it was found that the feed rate for obtaining the smallest particle size was 100.0 ml/min for this study.

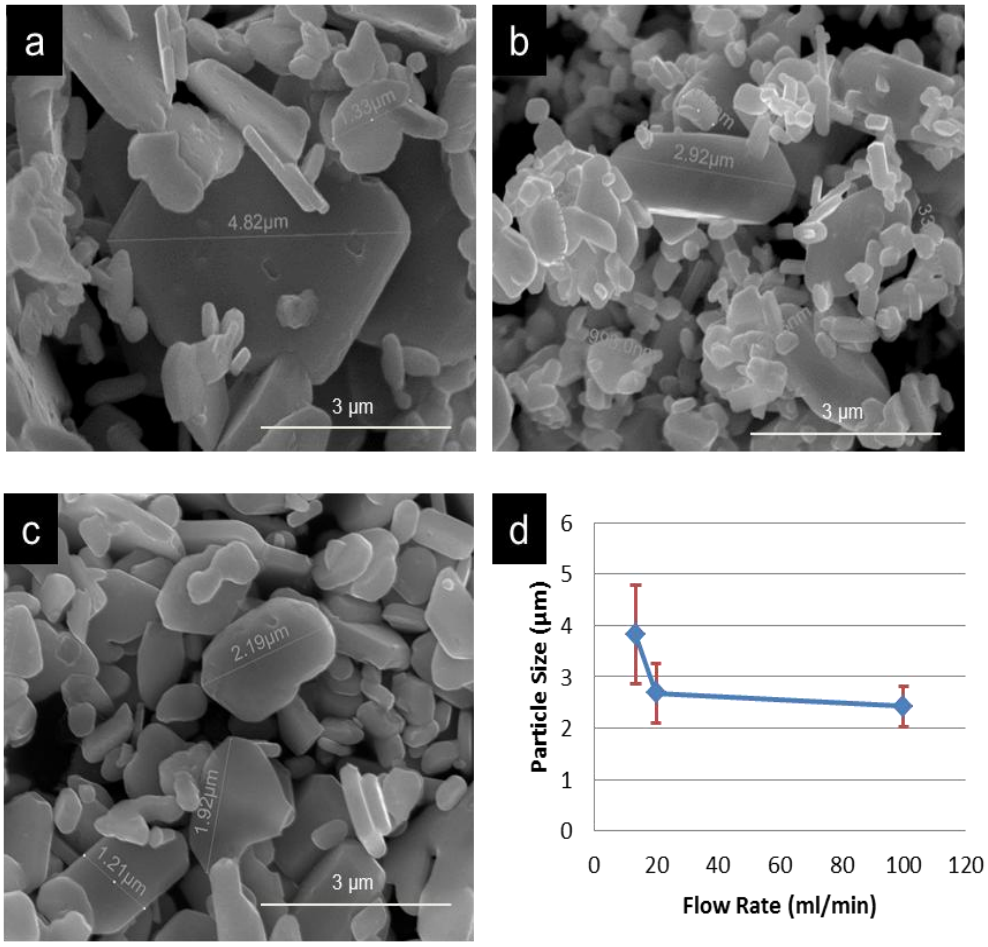

Figure 8 SEM images of AgO particles (a) SEM Image of the AgO for 10 ml/min addition rate of $AgNO_3$, (b) 20 ml/min addition rate of $AgNO_3$, (c) 100 ml/min addition rate of $AgNO_3$. (d) $AgNO_3$ feed rate and particle size relation (Temperature: 60 °C, $K_2S_2O_8$]/[NaOH] Mole Ratio: 0.18, Mixing Speed: 500 rpm, $AgNO_3$ Feed Rate: 100 ml/min).

4.1.4 Effect of $[K_2S_2O_8]$/ [NaOH] Mole Ratio on Particle Size

Once the sodium hydroxide (NaOH) and potassium persulfate ($K_2S_2O_8$) have been mixed to form a homogeneous mixture, $AgNO_3$ was added to the reaction vessel under continued mixing at 500 rpm and 60°C. The prepared mother solution was a strong base and it causes AgO particles to nucleate and precipitate. The preferred bases for use in this reaction were NaOH and $K_2S_2O_8$. The precipitated AgO was washed with pure water and dried at 65°C in vacuum oven. The drying temperature was specially kept under 100°C to prevent the conversion of AgO to Ag_2O.

Effects of $[K_2S_2O_8]$/ [NaOH] Mole Ratio on particle size and morphology were investigated. The samples were characterized by scanning electronic microscope (SEM) and X-ray powder diffraction (XRD). The relationship between the amount of NaOH used and purity of produced AgO was shown in Figure 9 (a). From the figure it can be seen after reaching 0.27 moles of NaOH, high purity AgO particles can be obtained. To investigate the relationship between AgO particle size and the ratio of moles of $[K_2S_2O_8]$/[NaOH], further experiments were carried on. Figure 9 (b) presents the variations on the size of the resulting silver oxide particles with varying $[K_2S_2O_8]$/[NaOH] mole ratio. Changing the $[K_2S_2O_8]$/[NaOH] mole ratio from 0.1 to 0.18, results an obvious change in particle size. In order to reach smaller particle sizes, $[K_2S_2O_8]$/[NaOH] mole ratio has to be kept not less than or higher than 0.15.

Varying the $[K_2S_2O_8]$/[NaOH] mole ratio values also made a significant influence on the properties of AgO particles. Figure 9 (c) shows the effect of mole ratio of $[K_2S_2O_8]$/[NaOH] on particle size distribution and distribution width of the prepared AgO particles. As expected, mean particle size considerably changes with respect to changes in mole ratio of $[K_2S_2O_8]$/[NaOH]. The median size ranges between 2.902 to 2.096, when $[K_2S_2O_8]$/[NaOH] mole ratio varies from 0.1 to 0.18. As shown in Figure 9 (c), when the $[K_2S_2O_8]$/[NaOH] mole ratio is lower than 0.15, the particle size increases from 2.096 to 2.902; when the $[K_2S_2O_8]$/[NaOH] mole ratio is higher than 0.15, the particle size increases from 2.096 to 2.426. It was found that $[K_2S_2O_8]$/[NaOH] mole ratio affected the morphologies of the product by means of different crystal growth rates. When the $[K_2S_2O_8]$/[NaOH] mole ratio was adjusted at 0.12, the results indicated that the particles exhibited diamond irregular flake-like morphology. At 0.15 $[K_2S_2O_8]$/[NaOH] mole ratio, as the value increased, relatively smaller and faceted particles were formed (Figure 9 (d)). Spherical particles of AgO were formed at 0.18 $K_2S_2O_8$/[NaOH] mole ratio. This phenomenon is a result of precipitation kinetics such as nucleation and growth rate of the particles. When the $[K_2S_2O_8]$/[NaOH] mole ratio is kept low, so the concentration in the reaction vessel and the supersaturation is also low. As a result, there are a few nuclei in the reaction solution. Because no more new nuclei form, the existing nuclei continue to grow and particle sizes increase. At higher $[K_2S_2O_8]$/[NaOH] mole ratio, the system of concentration is supersaturated; the probability of collisions between them increases, this time agglomeration of the particles occurs and particle size becomes larger again. So, the optimum $[K_2S_2O_8]$/[NaOH] mole ratio for this precipitation reaction is 0.15. Also, $[K_2S_2O_8]$/[NaOH] mole ratio of 0.15 have the smallest distribution width in all samples.

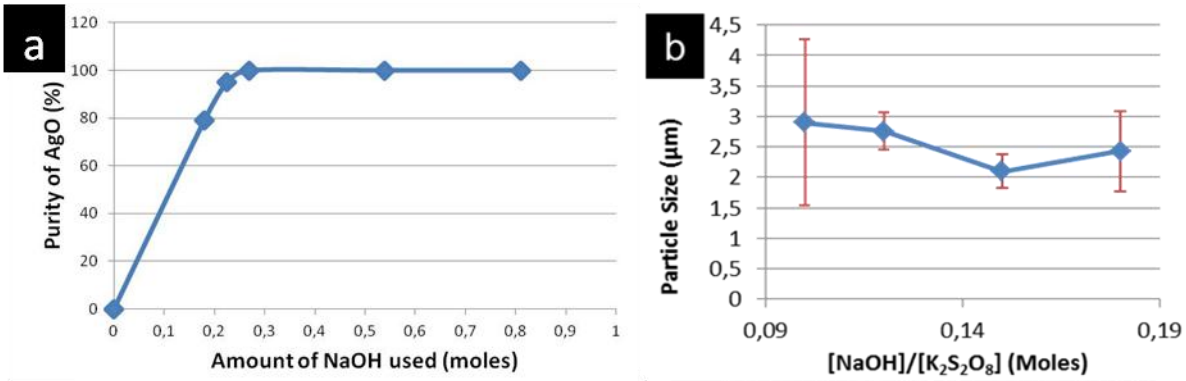

c

Mole Ratio of $[K_2S_2O_8]/[NaOH]$	Particle Size Distribution			Distribution Width (R)
	$D_{10/\mu m}$	$D_{50/\mu m}$	$D_{90/\mu m}$	
0.1	0.837	2.902	23.706	7.88
0.12	0.888	2.756	5.431	1.65
0.15	1.214	2.096	3.527	1.16
0.18	1.087	2.426	8.880	3.22

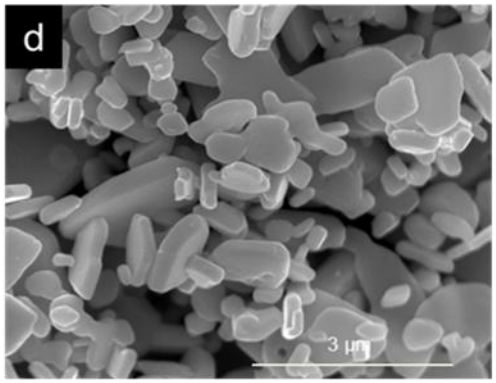

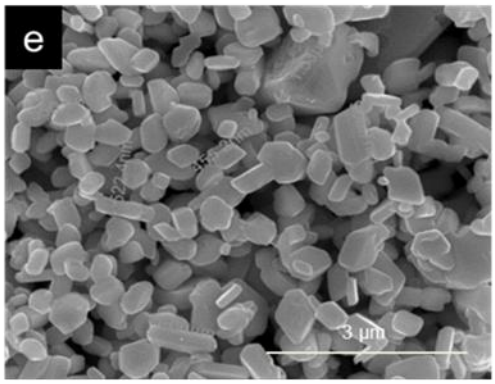

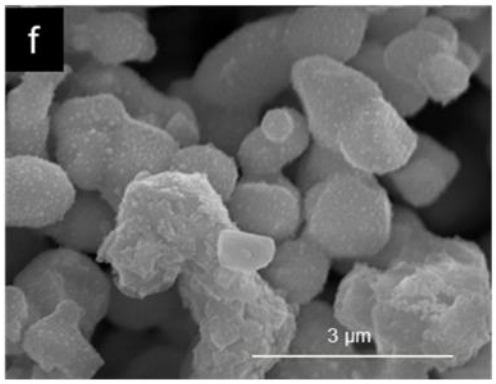

Figure 9 (a) Relationship of AgO purity with the amount of NaOH used (moles). (b) Relationship of AgO particle size with the ratio of moles of $[K_2S_2O_8]/[NaOH]$. (c) Comparison of mole ratio of $[K_2S_2O_8]/[NaOH]$ on particle size. SEM Image of the AgO particle produced with (d) 0.12 $[K_2S_2O_8]/[NAOH]$ mole ratio (e) 0.15 $[K_2S_2O_8]/[NaOH]$ mole ratio (f) 0.18 $[K_2S_2O_8]/[NAOH]$ mole ratio

4.1.5 Comparison of the Effect of the Different Surfactants on Particle Size

For battery applications, chemically stabilized particles with large surface areas are needed to reach high discharge rates. However, during the reaction depending on reduction kinetics, particles tend to grow and coalescence. Generally, surfactants are used to inhibit the coalescence of the particles. So, chemical reduction of AgO with using different surfactant chemistries was studied for the purpose of manufacturing products with uniform quality at large volumes.

The choice of an appropriate surfactant is one of the most critical parameter for the chemical reduction of AgO. Because growth process is controlled with the surfactant employed in the reaction vessel, it is possible to synthesize particles with different shapes and sizes depending on the targeted application.

Surfactants that are employed in this study are summarized in Figure 10 (a). Effect of each surfactant on particle size is studied between 0.01-1% surfactant concentration ranges. During the studies water miscible or water soluble organic surfactants were used. A homogeneous $AgNO_3$-Surfactant mixture was prepared to perform the reactions successfully. The comparison of the effect of the different surfactants for 0.1 % wt. concentration on particle size is presented in Figure 10 (b). It is obvious that in the presence of surfactants, particle size of AgO shows significant differences than that in the absence of a surfactant in the precipitation reaction. Also, it should be noted that the effect is not the same for each surfactant that is present in the reaction. In the presence of nonionic surfactants (PEG 400 and IGEPAL CA-630) mean particle size reaches maximum. At that surfactant concentration, PEG 400 and IGEPAL CA-630 are the surfactants that are showing the highest particle size with low uniformity and wide particle size distribution. The effect of anionic surfactants on AgO particle size is studied by running experiments in the presence of SDBS and CMC. The flat or broad curve indicates that the particle sizes are spread over a wide range of values. Also, the fluctuation on curves indicates a bimodal distribution of particle sizes. However, the effect of the CTAB on particle size is more significant and interesting. The sharpness of the plot gives a qualitative indication of the spread in particle size. This sharp peak shows that the particles are of similar size. From the experimental studies, it was understood that when 0.1% wt. concentration CTAB is added to reaction, particle size decreases sharply, and distribution becomes narrower as it is understood from smaller distribution width number from different from other surfactants studied (Figure 10). As a result, particle size in the presence of surfactants at 0.1% wt. concentration is as followed in decreasing order: PEG 400 > CMC > IGEPAL CA-630 > SDBS > CTAB.

a

Name	Type	Concentration Range (% wt.)
IGEPAL CA-630	Nonionic	0.01 – 1
PEG 400	Nonionic	0.01 – 1
CTAB	Cationic	0.01 – 1
SDBS	Anionic	0.01 – 1
CMC	Anionic	0.01 – 1

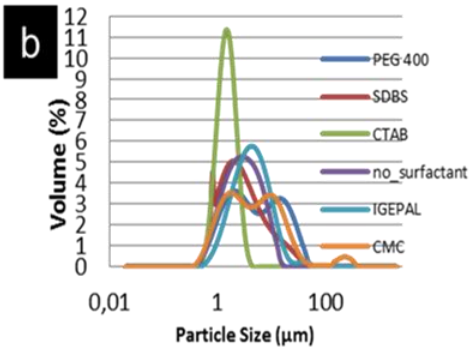

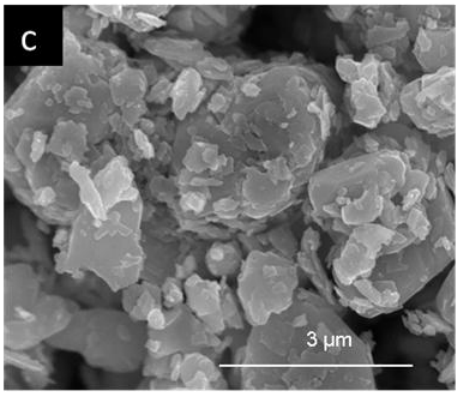

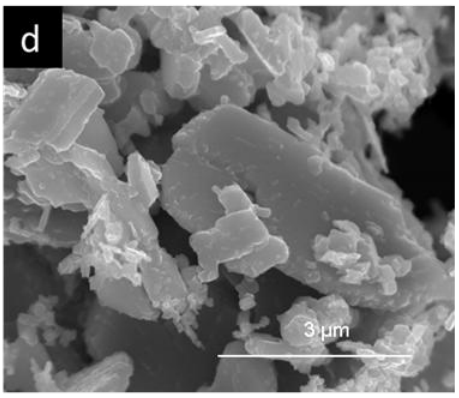

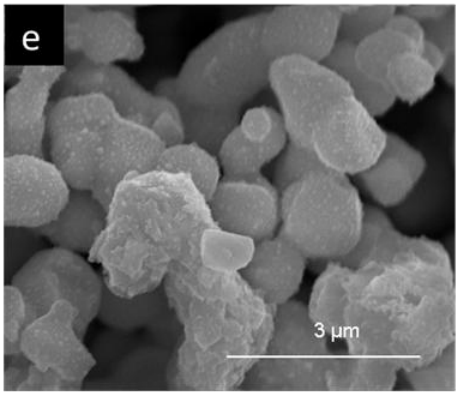

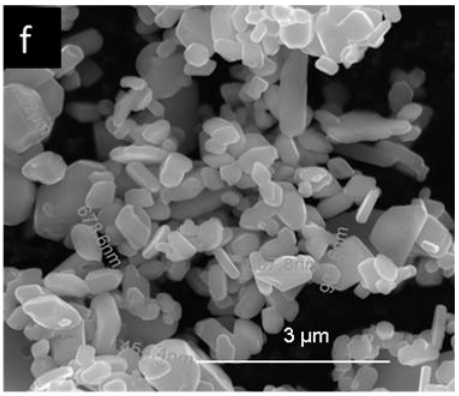

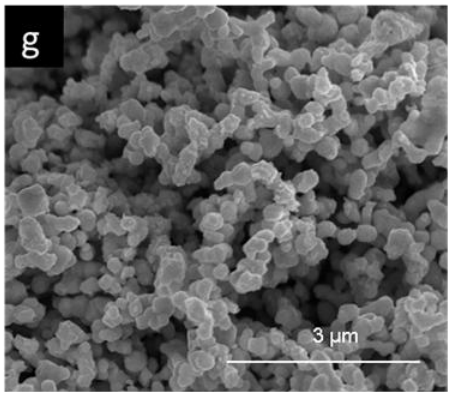

Figure 10 (a) Surfactants that are used during the experiments, (b) Comparison of effect of surfactants on particle size for 0.1 % wt. surfactant concentration. SEM Image of AgO powders for 0.1 % wt. (c) PEG 400, (d) CMC, (e) IGEPAL CA-630, (f) SDBS, (g) CTAB.

Figure 11 demonstrates the AgO particles produced from the use of various concentration of CTAB 0.03 M, 0.05 M, 0.1 M, 0.3 M, 0.5 M). The AgO formation is observed at all concentrations of CTAB; however, morphology yield and structural purity vary significantly with surfactant concentration. At very low concentrations such as 0.01% wt., no significant effect of the CTAB is observed and particle size still remains greater than 2.00 μm. Moreover, synthesized particles do not have uniformity at this surfactant concentration. The observation suggests that inadequate amount of surfactant exist in the media to direct nanosized particle formation. The production was improved considerably with the increase in surfactant concentration. The mean particle size of AgO is successfully stabilized and dropped less than 1.5 μm by 0.1% wt. CTAB concentration, which is determined as the optimum concentration for production of desired AgO particles. Because, at higher concentrations about 1.0 % wt., particles becomes unstable and the agglomeration cannot be inhibited. Also, the excess concentration of the CTAB causes impurities, and this can lead to performance loses of produced electrodes. This is most likely due to continue of the growth process with additional supply of surfactant and dissolution of some of the AgO particles to contributing to the further growth of particles and branching on their surface with a mechanism known as Oswald ripening. Therefore, the optimal amount of CTAB employed should preferably be around 0.1 % by weight of dissolved silver metal in the silver nitrate solution.

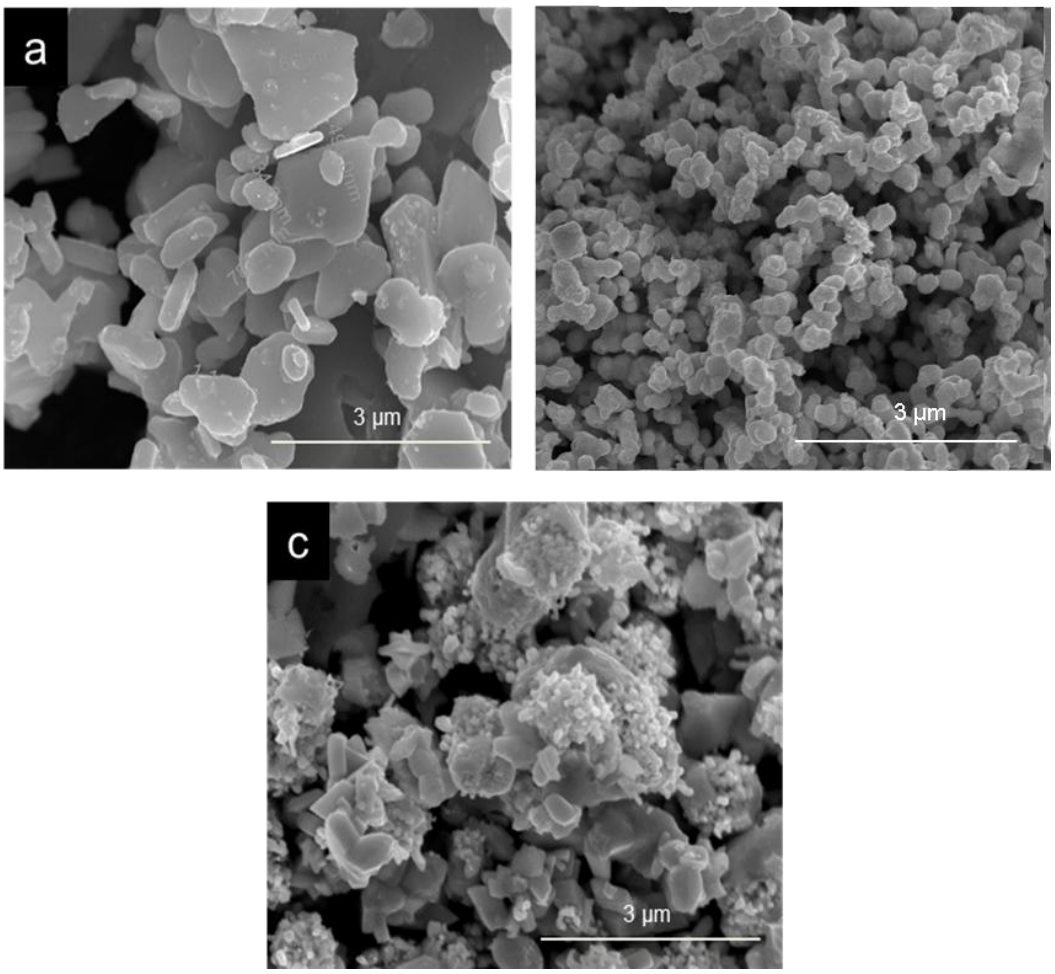

Figure 11 SEM Image of the AgO powders for (a) 0.01 % wt., (b) 0.1 % wt., and (c) 1 % wt. CTAB

4.1.6 Effect of the Sonocrystallization Process on Particle Size

After observing the effects of surfactants on mean particle size and particle size distribution, the studies are focused on understanding the effect of the sonocrystallization on morphology, structure and size of the particles. The experiments were performed on Syrris Atlas Sonolab system. The Atlas SonoLab system consisted of Syrris' Atlas Potassium Jacketed Vessel System, Prosonix proprietary ultrasonic flow cell, generator and pump. The accurate control of the overall system parameters was achieved with Atlas Software.

Ultrasonic treatment of reaction can be carried out in three different ways, including continuous, pulsed and initial insonation. Continuous insonation is preferred for producing many nuclei resulting in small crystals, whereas initial insonation produces finite nuclei which can be grown into large crystals. For producing nano-sized AgO, pulsed insonation is preferred because this method allows achieving a tailored crystal size. Because of the strong heating effects observed for insonation power outputs of 70 W and higher, experiments were only done with power outputs from 10 W to 60 W. For the sake of consistency the residence time in the reactor is referred to as insonation time for all experiments. Pulsed sonication is studied between 10 W to 60 W ranges and the effect of pulsed sonication during the reaction on particle size was monitored. In Figure 12 SEM images are given for AgO particles that are prepared by sonochemical method. When the applied power is changed from 10 to 60 W, different sizes and morphologies are obtained. As can be seen from Figure 12 (b), the application of 10 W insonation did not affect the particles' size obviously. Rather than nanoparticles, still micron-sized other shapes are formed. Figure 12 (b) shows relative large crystals with generally well defined faces surrounded by small crystals (<1 μm) with irregular shapes. This is mainly the result of insufficient amount of power application to the reaction media to support nanosized particle formation. The nano particle production was improved considerably with the increase in insonication power. At 30 W, the crystals are stacked on top of each other, but don't appear to be agglomerated (Figure 12 (c)). The smallest particle size (0.283 μm mean particle size) with uniform particle size distribution, and highest surface area was obtained at 30 W insonation power which is determined as the optimum power value for the synthesis of AgO nanoparticles. AgO of such a small particle size can produce both super high speed charge and discharge when it serves as the electrode material due to its large actual surface area. Sonocrystallization at 30 W during the reaction allows narrow particle size distributions by controlled nucleation. It can be concluded from Figure 11 (e) that advanced control of nucleation and growth rate results in very narrow particle size distribution. Also, high AgO wt. % is observed when the insonation power was kept at 30 W (Figure 11(f)). Increasing the power to 60 W leads to a significant increase in the diameter of nanoparticles and a change in the morphology of the produced particles. The characteristic faceted shape of AgO crystals was not observed and instead the dominant shapes appear to be irregular spherical particles (Figure 12 (d)).The SEM image shows that the faces were not well defined and agglomeration between crystals was observed. The effect of insonation in AgO forming is seen to be very pronounced for relatively medium power applications. A possible explanation for the increase in particle size is that, if the insonation power becomes too high the nuclei started to dissolve again. The dissolution of some of the AgO particles contributes to the further growth of particles and branching on their surface with a mechanism known as Oswald ripening. The optimum power is found to be 30 W and increasing the power results in increase of AgO particle size as shown in Figure 12 (a)).

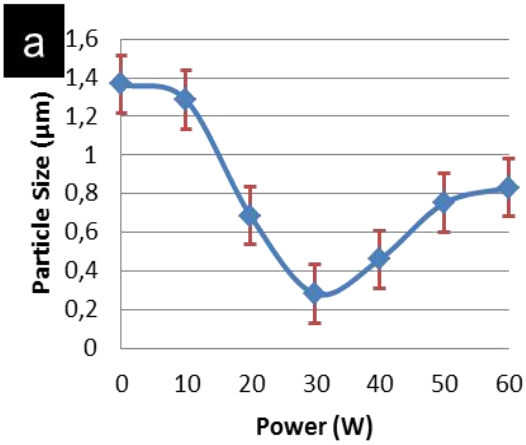

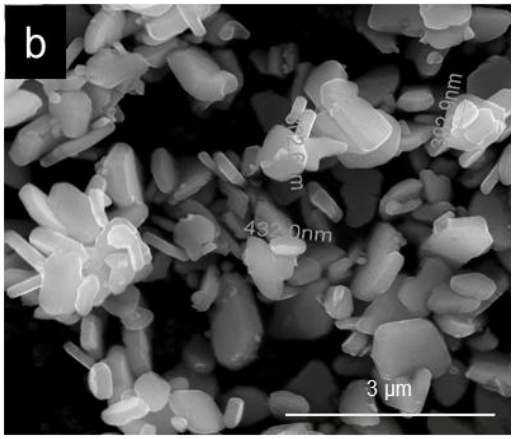

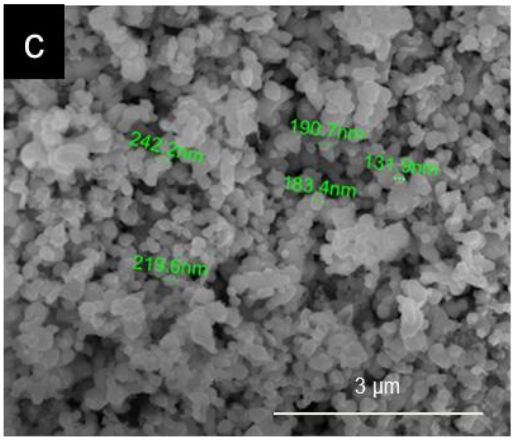

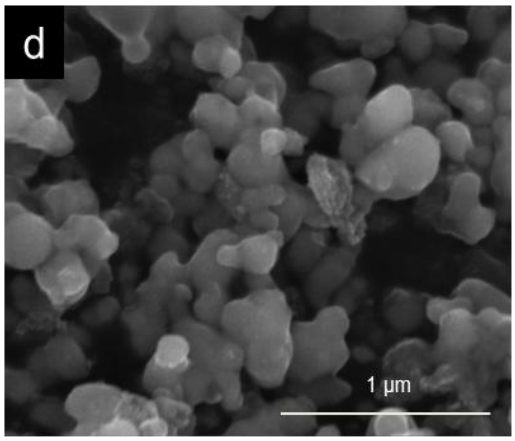

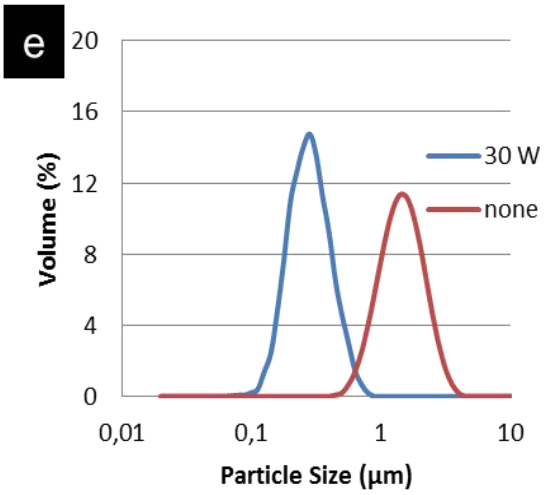

f

Power (W)	Surfactant Type	AgO (wt. %)	Ag_2O (wt. %)
30	IGEPAL CA-630	74.90	25.10
30	SDBS	84.13	15.87
30	CTAB	100.0	-

Figure 12 (a) Effect of sonocrystallization on particle size (Temperature: 60°C, $[K_2S_2O_8]$/[NaOH] Mole Ratio: 0.15, Mixing Speed: 500 rpm, $AgNO_3$ Feed Rate: 100 ml/min, CTAB Concentration: 0.1 % wt.). SEM Image of the AgO particles after (b) 10 W, (c) 30 W, (d) 60 W sonocrystallization process**.** (e) Particle size measurement results of chemically and sonochemically prepared AgO. (f) XRD results of sonochemically prepared AgO particles (30 W) with different surfactants.

The material was lastly characterized with XRD analysis. Figure 13 (a) and (b) represent the powder XRD patterns of the IGEPAL and CTAB capped AgO particles prepared by sonochemical route. The XRD study establishes the formation of highly crystalline AgO nanoparticles in the presence of pronounced narrow peaks. So, the material can be considered to exhibit symmetric ordering and should be characterized as crystalline. The test results in Figure 13 (a) shows the typical crystalline structure of AgO and Ag_2O based on Rietveld Refinement. The XRD pattern of the sample exhibits extra low intensity peaks of impurity phases compared to the AgO pattern. These diffraction peaks can be well assigned to a typical crystalline structure of Ag_2O according to Rietveld plot. The AgO content of the prepared powder was found to be 74.90 %, whereas the Ag_2O content of the powder was 25.10 %. Figure 13 (b) gives the XRD pattern of CTAB asssited synthesized AgO particles. No obvious reflection peaks from impurities were detected, and the AgO content of the powder is found to be 100 %. XRD profiles show that the nanoparticles synthesized with CTAB show high purity diffraction features when compared to that of the samples produced with IGEPAL. The peaks corresponding to Ag_2O phase showed up in AgO-IGEPAL sample, whereas these peaks disappeared in AgO-CTAB samples.

From the XRD analysis given in Figure 13 (c), it can be concluded that the addition of surfactants results in a reduced intensity of the diffraction peaks for the surfactant-free AgO samples, but still maintains the crystalline phase of the material. However, the increase or decrease in the peak intensity depends on the lattice orientation or rearrangement. Surfactants typically play crucial roles in the particle size and size distribution. The addition of surfactant as capping agent/structure directing agent in the synthesis produces monodispersed and small size nanoparticles. The nanoparticles with smaller size diffract X-rays weakly. In addition this significant decrease in the diameter of nanoparticles, a change in the morphology of the produced particles was observed. After the surfactant addition, the dominant shapes appear to be spherical particles rather than characteristic faceted shape of AgO crystals, which caused a shift in the diffraction pattern.

Because, the studies conducted in this thesis, will be used in battery manufacturing, adaptation of the method to mass production is of great importance. This laboratory scale sonocrystallization process can be scaled to pilot plant processes using the Prosonix Ltd. range of products. Therefore, the method descried here is a scalable and reproducible process with automated control of process parameters.

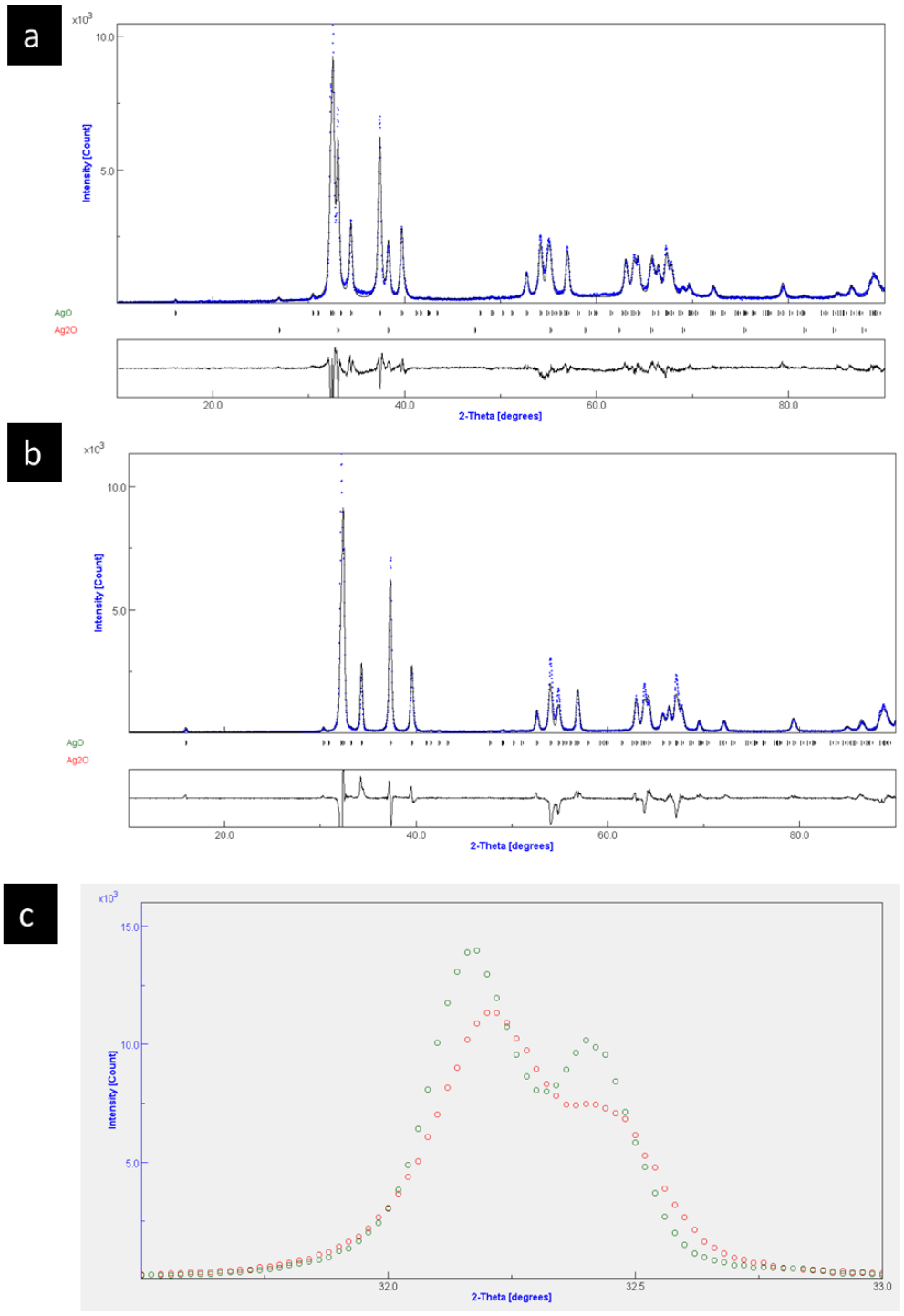

Figure 13 XRD patterns of divalent silver oxide nanopowder formed with different surfactants (a) 0.1 % wt. IGEPAL CA-630 (b) 0.1 % wt. CTAB. (c) Comparison of AgO-(200) peak (left) and AgO-(111) peak (right) of AgO nanoparticles synthesized with 0.1 % wt. CTAB (red line) and without surfactant (green line).

CHAPTER 5

CONCLUSION

The energy efficiency and capacity of the batteries can be improved by applying nanotechnological innovations to commercial batteries. The use of nanoparticles as electrode materials has made a significant improvement in battery performance due to their enhanced electrical and chemical properties. Nano-sized AgO cathode lead Zn-AgO batteries to reach even super high charge/discharge rates because of particles' considerably large surface area. The research pioneer of this study is to produce nano-sized divalent silver oxide particles with high speed charge/discharge ability as cathode active material for Zn-AgO battery. Nano size AgO powder was prepared through a surfactant aided sonochemical route. Parametric study was performed to examine the effect of reaction parameters such as reaction time, reaction temperature, and surfactant concentration on the quality of products. It was observed that these parameters play crucial roles on the morphology, yield and structural purity of the materials produced. Based on the data presented in this study, we can draw the following conclusions and insights for this reaction system:

- Thermodynamically stable AgO nanoparticles can be easily synthesized from the alkaline oxidation of $AgNO_3$ solution with $K_2S_2O_8$ and NaOH at 60^oC. Additionally, the optimum reaction time is observed as 120 min for the reactions carried out at 60 ^oC.

- Addition rate of $AgNO_3$ has a significant effect on residence time and monosized AgO can be synthesized by maintaining the addition rate, thus the residence time as short as possible.

- The mole ratio of $[K_2S_2O_8]$/[NaOH] is a dominant factor in determining the crystallite size of precipitates by means of different crystal growth rates. By keeping this ratio at 0.15, we obtained faceted AgO particles with the smallest particle size and narrow particle size distribution.

- Chemical reduction of AgO, both using water miscible and water soluble organic surfactant chemistries, was studied between 0.01-1% surfactant concentration ranges and the mean particle size of AgO is successfully stabilized and agglomeration can

be inhibited by 0.1% wt. CTAB concentration, which is determined as the optimum concentration for production of desired AgO particles.

- Advanced control of nucleation and growth rate can be achieved by pulsed insonation. Average particle size of 0.283 μm with uniform particle size distribution was obtained at 30 W insonation power which is determined as the optimum power value for the synthesis of AgO nanoparticles. The AgO content of the prepared powder was 100 % and powder particle size mainly distribute in the range of 100-300 nm. AgO belongs to simple monoclinic crystal system.

As a conclusion, surfactant aided sono-chemical precipitation method was investigated and the effect of process parameters on the produced AgO nanoparticle characteristics was studied in detail. This aided in an optimization of the precipitation parameters to produce AgO nanopowders with desired particle size, structural purity, and yield. The method reported is comparatively simple, cost-effective, and easy scale up process.

REFERENCES

[1] T. B. Reddy, *Linden's handbook of batteries*: McGraw-Hill Companies, 2010.

[2] G. Pistoia, *Battery operated devices and systems: From portable electronics to industrial products*: Elsevier Science, 2008.

[3] K. Gansky, "Rechargeable batteries applications handbook," Butterworth Heinemann, 2002.

[4] R. M. Dell, and D. A. J. Rand, *Understanding batteries*: Royal Society of Chemistry, 2001.

[5] C. Vincent, and B. Scrosati, *Modern Batteries 2nd Edition*: Butterworth-Heinemann, 1997.

[6] H. A. Kiehne, *Battery technology handbook*: CRC, 2003.

[7] M. Barak, *Electrochemical power sources: primary and secondary batteries*: Inst of Engineering & Technology, 1980.

[8] mpoweruk. http://www.mpoweruk.com/chemistries.htm.

[9] G. E. Products, *Rechargeable Batteries Applications Handbook*: Newnes, 1997.

[10] L. Gaines, "Secondary Silver-Zinc Battery Technology," *Journal of The Electrochemical Society*, vol. 116, no. 2, pp. 61C-67C, 1969.

[11] J. Skelton, and R. Serenyi, "Improved silver/zinc secondary cells for underwater applications," *Journal of power sources*, vol. 65, no. 1, pp. 39-45, 1997.

[12] D. F. Smith *et al.*, "New developments in very high rate silver oxide electrodes," *Journal of power sources*, vol. 65, no. 1, pp. 47-52, 1997.

[13] A. P. Karpinski *et al.*, "Silver based batteries for high power applications," *Journal of power sources*, vol. 91, no. 1, pp. 77-82, 2000.

[14] T. R. Crompton, *Battery reference book*: Newnes, 2000.

[15] P. Arora, and Z. Zhang, "Battery separators," *Chemical Reviews-Columbus*, vol. 104, no. 10, pp. 4419-4462, 2004.

[16] W. J. Ingram, *New technology batteries guide*: The Institute, 1998.

[17] M. Root, *The TAB Battery Book: An In-depth Guide to Construction, Design, and Use*: McGraw-Hill/TAB Electronics, 2010.

[18] A. Fleischer, and J. J. Lander, *Zinc-silver oxide batteries*, DTIC Document, 1971.

[19] E. Nakao, H. Yamazaki, and M. Hirooka, "Separator for an alkaline battery," Google Patents, 1987.

[20] S. U. Falk, and A. J. Salkind, *Alkaline storage batteries*: Wiley New York, 1969.

[21] S. P. Poa, and C. H. Wu, "A quantitative study of shape change in zinc secondary electrodes," *Journal of Applied Electrochemistry,* vol. 8, no. 5, pp. 427-436, 1978.

[22] J. S. Chen, F. R. McLarnon, and E. J. Cairns, "Investigation of low-zinc-solubility electrodes and electrolytes in zinc/silver oxide cells," *Journal of power sources,* vol. 39, no. 3, pp. 333-348, 1992.

[23] A. Charkey, "Sealed zinc secondary battery and zinc electrode therefor," Google Patents, 1995.

[24] B. Hariprakash, S. K. Martha, and A. K. Shukla, "Galvanostatic non-destructive characterization of alkaline silver–zinc cells," *Journal of power sources,* vol. 117, no. 1, pp. 242-248, 2003.

[25] I. F. Danzig, "Zinc electrode for use in rechargeable electrochemical cells," Google Patents, 1983.

[26] J. Garche *et al.*, *Encyclopedia of electrochemical power sources*: Academic Press, 2009.

[27] M. I. Gillibrand, L. Langrish, and G. R. Lomax, "Reaction in the silver zinc cell," *Journal of Applied Electrochemistry,* vol. 1, no. 1, pp. 9-17, 1971.

[28] J. P. Allen, D. O. Scanlon, and G. W. Watson, "Electronic structure of mixed-valence silver oxide AgO from hybrid density-functional theory," *Physical Review B,* vol. 81, no. 16, pp. 161103, 2010.

[29] T. P. Dirkse, D. DeWit, and R. Shoemaker, "Silver Oxide Electrode Processes," *Journal of The Electrochemical Society,* vol. 114, no. 12, pp. 1196-1200, 1967.

[30] S. P. Poa, and C. H. Wu, "The current distribution and shape change of zinc electrodes in secondary silver-zinc cells," *Journal of Applied Electrochemistry,* vol. 8, no. 6, pp. 491-501, 1978.

[31] R. E. F. Einerhand *et al.*, "Zinc electrode shape change II. Process and mechanism," *Journal of The Electrochemical Society,* vol. 138, no. 1, pp. 7-17, 1991.

[32] A. Charkey, "Zinc electrodes for secondary batteries," Google Patents, 1977.

[33] J. E. Casey Jr, "High performance zinc anode for battery applications," Google Patents, 1998.

[34] J. R. Serenyi, "Rechargeable alkaline silver-zinc cell with improved negative electrode," Google Patents, 1998.

[35] T. P. Dirkse, “The Silver Oxide Electrode,” *Journal of The Electrochemical Society,* vol. 106, no. 5, pp. 453-457, 1959.

[36] Y. Ye, “Elabd YA In Polymers for energy storage and delivery: Polyelectrolytes for batteries and fuel cells. Page, KA; Soles, CL; Runt,” *J. Eds*, pp. 233-251.

[37] R. Qadeer *et al.*, “Synthesis and characterization of silver (II) oxide,” *Journal of the Chemical Society of Pakistan,* vol. 21, no. 4, pp. 368, 2011.

[38] A. F. Wells, *Structural inorganic chemistry*: Clarendon Press Oxford, 1975.

[39] D. Tudela, “Silver (II) Oxide or Silver (I, III) Oxide?,” *Journal of Chemical Education,* vol. 85, no. 6, pp. 863, 2008.

[40] N. N. Greenwood, and A. Earnshaw, “Chemistry of the Elements,” 1984.

[41] "properties of divalent silver oxide," http://en.wikipedia.org/wiki/Silver(I,III)_oxide.

[42] K. Dunn, and V. Edwards-Jones, “The role of Acticoat with nanocrystalline silver in the management of burns,” *Burns: journal of the International Society for Burn Injuries,* vol. 30, pp. S1, 2004.

[43] A. D. Russell, F. R. C. Path, and W. B. Hugo, “7 Antimicrobial Activity and Action of,” *Progress in medicinal chemistry,* vol. 31, pp. 351, 1994.

[44] M. Ip *et al.*, “Antimicrobial activities of silver dressings: an in vitro comparison,” *Journal of Medical Microbiology,* vol. 55, no. 1, pp. 59-63, 2006.

[45] A. Petica *et al.*, “Colloidal silver solutions with antimicrobial properties,” *Materials Science and Engineering: B,* vol. 152, no. 1, pp. 22-27, 2008.

[46] M. Rai, A. Yadav, and A. Gade, “Silver nanoparticles as a new generation of antimicrobials,” *Biotechnology advances,* vol. 27, no. 1, pp. 76-83, 2009.

[47] J. S. Kim *et al.*, “Antimicrobial effects of silver nanoparticles,” *Nanomedicine: Nanotechnology, Biology and Medicine,* vol. 3, no. 1, pp. 95-101, 2007.

[48] P. Li *et al.*, “Synergistic antibacterial effects of β-lactam antibiotic combined with silver nanoparticles,” *Nanotechnology,* vol. 16, no. 9, pp. 1912, 2005.

[49] F. Martinez-Gutierrez *et al.*, “Synthesis, characterization, and evaluation of antimicrobial and cytotoxic effect of silver and titanium nanoparticles,” *Nanomedicine: Nanotechnology, Biology and Medicine,* vol. 6, no. 5, pp. 681-688, 2010.

[50] F. Di Fonzo *et al.*, "MATERIAL OF NANO-AGGREGATES OF TETRASILVER TETROXIDE," WO Patent WO/2008/120,259, 2008.

[51] W. Zhang, X. Qiao, and J. Chen, “Synthesis of silver nanoparticles—Effects of concerned parameters in water/oil microemulsion,” *Materials Science and Engineering: B,* vol. 142, no. 1, pp. 1-15, 2007.

[52] E. Stura, and C. Nicolini, “New nanomaterials for light weight lithium batteries,” *Analytica chimica acta,* vol. 568, no. 1, pp. 57-64, 2006.

[53] K. Murakami *et al.*, "Divalent silver oxide for use in primary cell and manufacturing method thereof," Google Patents, 1980.

[54] D. F. Smith, and C. Brown, “Aging in chemically prepared divalent silver oxide electrodes for silver/zinc reserve batteries,” *Journal of power sources,* vol. 96, no. 1, pp. 121-127, 2001.

[55] H. T. Liu, X. Xia, and Z. P. Guo, “A novel silver oxide electrode and its charge–discharge performance,” *Journal of applied electrochemistry,* vol. 32, no. 3, pp. 275-279, 2002.

[56] M. Jansen, and B. Standke, "Pure silver (III) oxide," Google Patents, 1988.

[57] K. N. Brown, "ARGENTOUS OXIDE," Google Patents, 1961.

[58] Z. Yan, R. Bao, and D. B. Chrisey, “Generation of Ag2O Micro-/Nanostructures by Pulsed Excimer Laser Ablation of Ag in Aqueous Solutions of Polysorbate 80,” *Langmuir,* vol. 27, no. 2, pp. 851-855, 2010.

[59] J. A. McMillan, “Higher Oxidation States of Silver,” *Chemical Reviews,* vol. 62, no. 1, pp. 65-80, 1962.

[60] K. Harigae, and Y. Shoji, "Fine-grain silver oxide powder," Google Patents, 2007.

[61] Y. Sun *et al.*, “Uniform silver nanowires synthesis by reducing AgNO3 with ethylene glycol in the presence of seeds and poly (vinyl pyrrolidone),” *Chemistry of Materials,* vol. 14, no. 11, pp. 4736-4745, 2002.

[62] J. N. Solanki, and Z. V. P. Murthy, “Controlled Size Silver Nanoparticles Synthesis with Water-in-Oil Microemulsion Method: A Topical Review,” *Industrial & Engineering Chemistry Research,* vol. 50, no. 22, pp. 12311-12323, 2011.

[63] Z. Li, Y. Wang, and Q. Yu, “Significant Parameters in the Optimization of Synthesis of Silver Nanoparticles by Chemical Reduction Method,” *Journal of materials engineering and performance,* vol. 19, no. 2, pp. 252-256, 2010.

[64] G. M. Berube, and G. Banerjee, "Nanosized silver oxide powder," Google Patents, 2007.

[65] K. C. Song *et al.*, “Preparation of colloidal silver nanoparticles by chemical reduction method,” *Korean Journal of Chemical Engineering,* vol. 26, no. 1, pp. 153-155, 2009.

[66] S. T. Hussain, and M. Mazhar, "Novel method of manufacture of silver oxide nano particles," Google Patents, 2007.

[67] S. Banerjee, A. K. Maity, and D. Chakravorty, “Quantum confinement effect in heat treated silver oxide nanoparticles,” *Journal of Applied Physics,* vol. 87, no. 12, pp. 8541-8544, 2000.

[68] D. D. Evanoff Jr, and G. Chumanov, “Size-controlled synthesis of nanoparticles. 1.“Silver-only” aqueous suspensions via hydrogen reduction,” *The Journal of Physical Chemistry B,* vol. 108, no. 37, pp. 13948-13956, 2004.

[69] D. Ghosh, and S. Dasgupta, “Synthesis of Submicron Silver Powder by the Hydrometallurgical Reduction of Silver Nitrate with Hydrazine Hydrate and a Thermodynamic Analysis of the System,” *Metallurgical and Materials Transactions B,* vol. 39, no. 1, pp. 35-45, 2008.

[70] S. Chen, and D. L. Carroll, “Synthesis and characterization of truncated triangular silver nanoplates,” *Nano letters,* vol. 2, no. 9, pp. 1003-1007, 2002.

[71] K. C. Chung *et al.*, "PROCESS FOR PREPARATION OF SILVER OXIDE," WO Patent 2,009,072,820, 2009.

[72] V. Scatturin, P. L. Bellon, and A. J. Salkind, “The structure of silver oxide determined by means of neutron diffraction,” *Journal of The Electrochemical Society,* vol. 108, no. 9, pp. 819-822, 1961.

[73] A. N. Mansour, and S. Dallek, “A new method for the quantitative analysis of silver oxide cathodes,” *Journal of The Electrochemical Society,* vol. 137, no. 5, pp. 1467-1471, 1990.

[74] T. Hoar, and J. Schulman, “Transparent water-in-oil dispersions: the oleopathic hydro-micelle,” *Nature,* vol. 152, pp. 102-103, 1943.

[75] Y. Hattori, and K. Waki, "Nanoparticle coated material and production method of same," Google Patents, 2005.

[76] K. V. P. M. Shafi *et al.*, “Sonochemical preparation of nanosized amorphous NiFe2O4 particles,” *The Journal of Physical Chemistry B,* vol. 101, no. 33, pp. 6409-6414, 1997.

[77] S. Sakohara, M. Ishida, and M. A. Anderson, “Visible luminescence and surface properties of nanosized ZnO colloids prepared by hydrolyzing zinc acetate,” *The Journal of Physical Chemistry B,* vol. 102, no. 50, pp. 10169-10175, 1998.

[78] T. Maruyama, and J. Shionoya, “Zinc oxide thin films prepared by chemical vapour deposition from zinc acetate,” *Journal of materials science letters,* vol. 11, no. 3, pp. 170-172, 1992.

[79] M. Brookshier, C. Chusuei, and D. Goodman, “Control of CuO particle size on SiO2 by spin coating,” *Langmuir,* vol. 15, no. 6, pp. 2043-2046, 1999.

[80] M. Verelst *et al.*, “Synthesis and characterization of CoO, Co3O4, and mixed Co/CoO nanoparticules,” *Chemistry of materials,* vol. 11, no. 10, pp. 2702-2708, 1999.

[81] K. S. Suslick, “The chemical effects of ultrasound,” *Scientific American*, vol. 260, no. 2, pp. 80-86, 1989.

[82] Y. Sun, and Y. Xia, “Shape-controlled synthesis of gold and silver nanoparticles,” *Science*, vol. 298, no. 5601, pp. 2176-2179, 2002.

[83] T. Arita *et al.*, *Divalent silver oxide for use in primary cell and manufacturing method thereof*, 1981.

[84] "Sonochemical Reaction and Synthesis," http://www.hielscher.com/ultrasonics/sonochem_01.htm.

[85] N. Lyczko *et al.*, “Effect of ultrasound on the induction time and the metastable zone widths of potassium sulphate,” *Chemical Engineering Journal*, vol. 86, no. 3, pp. 233-241, 2002.

[86] I. Nishida, “Precipitation of calcium carbonate by ultrasonic irradiation,” *Ultrasonics Sonochemistry*, vol. 11, no. 6, pp. 423-428, 2004.

[87] M. D. Luque de Castro, and F. Priego-Capote, “Ultrasound-assisted crystallization (sonocrystallization),” *Ultrasonics sonochemistry*, vol. 14, no. 6, pp. 717-724, 2007.

[88] S. Kim, C. Wei, and S. Kiang, “Crystallization process development of an active pharmaceutical ingredient and particle engineering via the use of ultrasonics and temperature cycling,” *Organic process research & development*, vol. 7, no. 6, pp. 997-1001, 2003.

[89] K. V. P. M. Shafi *et al.*, “Olympic ring formation from newly prepared barium hexaferrite nanoparticle suspension,” *The Journal of Physical Chemistry B*, vol. 103, no. 17, pp. 3358-3360, 1999.

[90] Y. Zhu *et al.*, “Sonochemical synthesis of titania whiskers and nanotubes,” *Chem. Commun.*, no. 24, pp. 2616-2617, 2001.

[91] P. Jeevanandam, Y. Koltypin, and A. Gedanken, “Synthesis of nanosized á-nickel hydroxide by a sonochemical method,” *Nano Letters*, vol. 1, no. 5, pp. 263-266, 2001.

[92] S. Avivi *et al.*, “Sonochemical hydrolysis of Ga3+ ions: synthesis of scroll-like cylindrical nanoparticles of gallium oxide hydroxide,” *Journal of the American Chemical Society*, vol. 121, no. 17, pp. 4196-4199, 1999.

[93] S. Avivi, Y. Mastai, and A. Gedanken, “A new fullerene-like inorganic compound fabricated by the sonolysis of an aqueous solution of TlCl3,” *Journal of the American Chemical Society*, vol. 122, no. 18, pp. 4331-4334, 2000.

[94] C. Y. Jimmy *et al.*, “Preparation of highly photocatalytic active nano-sized TiO2 particles via ultrasonic irradiation,” *Chemical Communications*, no. 19, pp. 1942-1943, 2001.

[95] D. Qian, J. Z. Jiang, and P. L. Hansen, “Preparation of ZnO nanocrystals via ultrasonic irradiation,” *Chemical communications*, no. 9, pp. 1078-1079, 2003.

[96] S.-H. Jung *et al.*, "Sonochemical preparation of shape-selective ZnO nanostructures," *Crystal growth and design,* vol. 8, no. 1, pp. 265-269, 2007.

[97] H. M. Xiong *et al.*, "Sonochemical synthesis of highly luminescent zinc oxide nanoparticles doped with magnesium (II)," *Angewandte Chemie International Edition,* vol. 48, no. 15, pp. 2727-2731, 2009.

[98] D. Zhang *et al.*, "Synthesis of CeO2 nanorods via ultrasonication assisted by polyethylene glycol," *Inorganic chemistry,* vol. 46, no. 7, pp. 2446-2451, 2007.

[99] C.-J. Mao *et al.*, "Sonochemical route for self-assembled V2O5 bundles with spindle-like morphology and their novel application in serum albumin sensing," *The Journal of Physical Chemistry B,* vol. 110, no. 30, pp. 14709-14713, 2006.

[100] D. P. Dutta *et al.*, "Indium oxide and europium/dysprosium doped indium oxide nanoparticles: sonochemical synthesis, characterization, and photoluminescence studies," *The Journal of Physical Chemistry C,* vol. 112, no. 17, pp. 6781-6785, 2008.

[101] M. Sivakumar *et al.*, "Fabrication of zinc ferrite nanocrystals by sonochemical emulsification and evaporation: observation of magnetization and its relaxation at low temperature," *The Journal of Physical Chemistry B,* vol. 110, no. 31, pp. 15234-15243, 2006.

[102] J. Geng *et al.*, "Hollow PbWO4 nanospindles via a facile sonochemical route," *Inorganic chemistry,* vol. 45, no. 20, pp. 8403-8407, 2006.

[103] J. Geng *et al.*, "Sonochemical synthesis of PbWO4 crystals with dendritic, flowery and star-like structures," *Nanotechnology,* vol. 17, no. 10, pp. 2614, 2006.

[104] J. Geng *et al.*, "One-dimensional BiPO4 nanorods and two-dimensional BiOCl lamellae: Fast low-temperature sonochemical synthesis, characterization, and growth mechanism," *Inorganic chemistry,* vol. 44, no. 23, pp. 8503-8509, 2005.

[105] D. P. Dutta, R. Ghildiyal, and A. K. Tyagi, "Luminescent properties of doped zinc aluminate and zinc gallate white light emitting nanophosphors prepared via sonochemical method," *The Journal of Physical Chemistry C,* vol. 113, no. 39, pp. 16954-16961, 2009.

[106] M. M. Mdleleni, T. Hyeon, and K. S. Suslick, "Sonochemical synthesis of nanostructured molybdenum sulfide," *Journal of the American chemical society,* vol. 120, no. 24, pp. 6189-6190, 1998.